Higher Dimension Quantum Entanglement Generators

KAITLIN N. SMITH and MITCHELL A. THORNTON, Southern Methodist University, USA

Quantum information processing and communication techniques rely heavily upon entangled quantum states, and this dependence motivates the development of methods and systems to generate entanglement. Much research has been dedicated to state preparation for radix-2 qubits, and due to the pursuit of entangled states, the Bell state generator and its generalized forms where the number of entangled qubits is greater than two have been defined. In this work, we move beyond radix-2 and propose techniques for quantum state entanglement in high-dimensional systems through the generalization of the binary bipartite entanglement states. These higher-radix quantum informatic systems are composed of n quantum digits, or qudits, that are each mathematically characterized as elements of an r-dimensioned Hilbert vector space where $r > 2$. Consequently, the wave function is a time-dependent state vector of dimension r^n. The generalization of the binary controlled-NOT to the controlled-modulo-addition gate, the concept of partial versus maximal entanglement, and architectures for generating higher-radix entangled states for the partial and maximal case are all presented.

CCS Concepts: • **Hardware → Quantum computation**;

Additional Key Words and Phrases: Quantum entanglement, quantum information processing, qudits

ACM Reference format:
Kaitlin N. Smith and Mitchell A. Thornton. 2019. Higher Dimension Quantum Entanglement Generators. *J. Emerg. Technol. Comput. Syst.* 16, 1, Article 3 (October 2019), 21 pages.
https://doi.org/10.1145/3345501

1 INTRODUCTION

The concept of representing, processing, and transmitting information through the use of quantum electrodynamic theory has been considered for several decades. However, the emergence of generalized quantum communication and computing systems as a mainstream technology, while seemingly closer than ever, has continued to remain elusive [7]. In addition to generalized quantum computing, systems and methods have been devised that are of a more specialized nature such as quantum cryptography and key distribution (QKD) [3, 22], sublinear complexity searching [13], true random number generators (TRNG) based upon quantum sources [4], quantum radar [16], quantum tomography [6, 21], quantum linear equation solvers [14], and others. In most of

Authors' address: K. N. Smith and M. A. Thornton, Southern Methodist University, Quantum Informatics Research Group, Dallas, TX, 75275; emails: {knsmith, mitch}@smu.edu.

1550-4832/2019/10-ART3 $15.00
https://doi.org/10.1145/3345501

these applications, one phenomenon that is necessarily exploited is that of entanglement. From a qualitative and non-rigorous perspective, entanglement is the characteristic of two or more quantum information carriers coupled together into a single subsystem such that operations performed on one of the carriers also affects the other(s). Entanglement is one of the unique characteristics resulting from the theory of quantum mechanics that is both non-intuitive and heavily exploited in quantum information processing (QIP) algorithms.

Conventional information processing technology is overwhelmingly based upon radix-2, or binary, switching algebras, and the most commonly used measure of information is the "bit." It is well-known, however, that higher-radix systems offer more information content per fundamental representational unit, or "digit" [17]. More precisely, an information processing system based upon a radix-r system allows for $log_2(r)$ bits of information to be represented per digit. Despite this higher-radix advantage, the rapid size decrease in transistors has caused the binary radix to continue to prevail, since transistor-based information processing circuits are predominantly in the form of voltage-mode devices. The increasingly smaller feature sizes and the corresponding and necessarily smaller rail voltage levels result in noise margins that cause higher-valued radices to be impractical in modern electronic information processing circuits. This happens because the benefits afforded by increasing the overall number of small transistors per unit of area in conventional electronic CPUs outweighs those that could potentially be realized through the use of larger transistors that are enabled to switch among multiple voltage levels in a higher-radix implementation. As a consequence, radix-2 or binary logic dominates in modern electronic devices under the classical computational models due to voltage level switching and small noise margins.

The use of higher-radix systems for the representation and processing of information in quantum information science (QIS) is potentially viable and offers advantages in terms of the amount of information that can be represented per system element. This observation provides motivation for the development of QIS systems that utilize quantum digits, or "qudits," rather than the more commonly considered quantum bits, or "qubits." This motivation includes a consideration of higher-radix QIS applications that depend on qudit entanglement. The remainder of this article focuses on the generation of entangled qudits and describes theoretical results and methods for the generation of higher-radix entangled states. Higher-radix entanglement [11] as well as methods for qudit quantum state generation have been considered in the past [25], but this work differs by presenting the single- and multi-qudit operators required to entangle quantum states, using the structure of bipartite binary entanglement generators as inspiration. The end result of this work is a generalized circuit structure that can be implemented in QIP algorithms to create varying degrees of higher-radix entanglement.

Quantum entanglement is an enabling property in many algorithms and communications schemes. For example, quantum key distribution (QKD) is dependent on the ability to generate entangled states. Furthermore, entanglement is a key phenomenon that is present inside many well-known binary quantum algorithms such as Shor's algorithm. Thus, for higher-radix QIP to become viable, it is important to determine methods to generate entanglement for higher-radix systems such as those described here. We focus on generalizations of the binary bipartite entanglement generators such as Bell generators and the multi-qubit GHZ generators for the higher-radix case. Our results provide a description of how higher-radix entanglement generators can be constructed from realizable physical components including the Chrestenson and controlled-modulo-addition operators.

This article will proceed as follows: Key concepts about QIP needed to understand the motivation of this work can be found in Section 2. In Section 3, the important operators used to create entanglement are presented and defined. This section includes the characterization of the

single- and multi-input entanglement gates for the radix-2 case and their generalization into a higher-radix form. Novel theoretical methods for generating partial and full entanglement for higher-dimension quantum systems are found in Section 4. Radix-3 example systems are implemented in Section 4 to demonstrate how entangled quantum states are produced by the generator circuits that are disclosed. Finally, Section 5 provides a summary of the work as well as conclusions.

2 QUANTUM THEORY CONCEPTS

2.1 Quantum Information

The most commonly used physical systems for quantum information are elements that have two distinct basis states. Due to the fact that the carriers have two distinct basis states, they carry information that is mathematically represented as a quantum bit, or qubit, by assigning each of the basis states to one of two orthonormal vectors. Quantum information can also be represented with carriers that exhibit quantum mechanical behavior over a non-binary basis set [8]. Mathematically, a higher-radix system can be characterized with a set of basis vectors that span a Hilbert vector space of dimension $r > 2$ in terms of qudits rather than the binary ($r = 2$) case of qubits. An example application for higher-radix QIP is QKD [1, 15, 20].

Qubits are the most commonly implemented units of information in QIP. As a result, methods for automatically generating arbitrary radix-2 quantum state have been considered, yet the general problem of logic synthesis to produce a cascade of known operators remains a research problem. In terms of generating arbitrary quantum states, a recent method for the binary case is given in Reference [19], yet the result is in terms of controlled rotation gates with arbitrary angles of rotation and not in terms of actual operators that are known to be fabricated in some technology.

As an example of higher-radix QIP, a radix-3 system consists of qudits expressed mathematically as a linear combination of three orthonormal basis vectors, $|0_3\rangle$, $|1_3\rangle$, and $|2_3\rangle$. In this case, the basis vectors span a three-dimensional Hilbert space. A general radix-3 qudit, $|\phi_3\rangle$ may be expressed mathematically as $|\phi_3\rangle = a_0|0_3\rangle + a_1|1_3\rangle + a_2|2_3\rangle$. The set of radix-3 computational basis vectors are explicitly denoted as $|0_3\rangle = [\,1 \quad 0 \quad 0\,]^{\mathrm{T}}$, $|1_3\rangle = [\,0 \quad 1 \quad 0\,]^{\mathrm{T}}$, and $|2_3\rangle = [\,0 \quad 0 \quad 1\,]^{\mathrm{T}}$. A quantum information system composed of two radix-3 qudits is formulated in the same manner as that of a multi-qubit system through use of the tensor product.

In general, the form of a single qudit for an arbitrary radix, r, is given by

$$|\phi_r\rangle = \sum_{i=0}^{r-1} a_i |i_r\rangle. \tag{1}$$

Additionally, it is also the case that the a_i in Equation (2) are complex-valued quantities that satisfy

$$\sum_{i=0}^{r-1} |a_i|^2 = 1. \tag{2}$$

2.2 Quantum Superposition

One advantage of QIP as compared to conventional information technology (IT) is that the state of a qubit can express non-zero components of both $|0_2\rangle$ and $|1_2\rangle$ simultaneously. This is the characteristic of "quantum superposition." In general, a QIP system of radix-r qudits can also exhibit superposition. Superposition enables the processing of multiple valuations of information in a single quantum computation. Mathematically, superposition is expressed by the presence of two or more basis vector coefficients, a_i, having non-zero values.

Example 2.1 (Radix-3 Superposition). Consider a radix-3 qudit defined as a linear combination of the three computational basis vectors, $|0_3\rangle$, $|1_3\rangle$, and $|2_3\rangle$. The radix-3 qudit is, in general, a superposition of these three basis states in the form of

$$|\phi_3\rangle = a_0|0_3\rangle + a_1|1_3\rangle + a_2|2_3\rangle = [\, a_0 \quad a_1 \quad a_2 \,]^{\mathrm{T}}. \tag{3}$$

The coefficients a_0, a_1, and a_2 are referred to as the "probability amplitudes" of the qudit $|\phi_3\rangle$ in accordance with the Born rule [5]. In Equation (3), a_0, a_1, and a_2 are complex values $c \in \mathbb{C}$, such that $c = x + iy$ where i is the imaginary number satisfying $i^2 = -1$. Furthermore, $\langle\phi_3|\phi_3\rangle = a_0^* a_0 + a_1^* a_1 + a_2^* a_2 = 1$.

Definition 2.2 (Maximal Superposition). When the probability amplitudes are all non-zero and the square of their magnitudes are the same value, the qubit or qudit is said to be *maximally superimposed* or is in *maximal superposition* with respect to some basis set. Practically, this means that the qudit is equally likely to be measured as being in a state that is equivalent to any of the possible basis vectors. Multiple qubits or qudits may demonstrate states of maximal superposition.

Achieving maximal superposition is a very important operation and is one that is typically achieved as one of the very first operations in many quantum computing algorithms or processing flows.

2.3 Quantum Operations

Mathematically, a QIP task is modeled as $|\phi_r(t_n)\rangle = \mathbf{U}|\phi_r(t_0)\rangle$. This represents the quantum state $|\phi_r\rangle$ evolving over a time period $t_n - t_0$ in accordance with the operations represented by $\mathbf{U}$. In general, $\mathbf{U}$ is a product of known operators with their own transformation matrices that can be realized in some technology. We represent these operators as $\mathbf{U}_i$. Thus, a QIP task that is synthesized into a known set of k operators is modeled as $|\phi_r(t_n)\rangle = [\mathbf{U_k U_{k-1}} \cdots \mathbf{U}_1]|\phi_r(t_0)\rangle$. Each particular transformation matrix $\mathbf{U}_i$ is representative of a QIP "circuit" or "gate."

When considering radix-r quantum operations, or gates, the transformation matrices will always be square matrices that are a power of r in dimension. Therefore, radix-3 qudit operations will be of size $3^n \times 3^n$, where the power, n, indicates the number of qudits.

2.4 Entanglement

When a set of quantum particles or entities are entangled, their behavior is considered as a composite system, since operations or observations performed on one element directly affect the other entangled elements. A given element within an entangled group cannot be described or characterized independently, since its properties are influenced by other elements within the entangled group.

Example 2.3 (Entanglement of a Qubit Pair). Consider two qubits $|\alpha_2\rangle$ and $|\beta_2\rangle$ that are entangled in the form $|\alpha\beta_2\rangle = a_{00}|00_2\rangle + a_{11}|11_2\rangle$. It is clear that $|\alpha\beta_2\rangle$ cannot be expressed as a product of $|\alpha_2\rangle$ and $|\beta_2\rangle$. The inability to factor a quantum state into distinct subsets is characteristic of entanglement. In this example, if the particle carrying the $|\alpha_2\rangle$ state is measured, the probability that $|0_2\rangle$ is observed is $|a_{00}|^2$. The amazing result is that such a measurement also causes the other entangled particle, the carrier of $|\beta_2\rangle$, to also collapse into $|0_2\rangle$.

The phenomenon described in Example 2.3 was accused of violating the special theory of relativity by Einstein et al. in their seminal paper [10], since the two entangled particles can be separated by a large physical distance and still exhibit this behavior. Hence, such entangled pairs are sometimes referred to as "EPR pairs" or "EPR states" and are the basis of techniques in QKD and quantum teleportation [18].

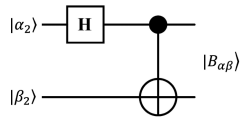

Fig. 1. Bell state generator.

Definition 2.4 (Maximal Entanglement). A quantum state is entangled whenever the state, such as the EPR pair $|\alpha\beta_2\rangle$ from Example 2.3, cannot be decomposed into a product of its members, $|\alpha\beta_2\rangle \neq |\alpha_2\rangle \otimes |\beta_2\rangle$. When the coefficients of an entangled quantum state have equal and non-zero values of squared magnitude for basis states, the quantum information is *maximally entangled*. A quantum state composed of two or more qubits or qudits is maximally entangled when each of the possible outcomes of an observation are equally likely, and the outcome quantum state demonstrates the following:

(1) measurement of a single unit in the entangled pair causes the other entangled qubit(s) or qudit(s) to collapse to a basis state without being directly measured or observed, and
(2) the basis state of the other entangled qubit(s) or qudit(s) is uniquely known by inference due only to the knowledge gained by observation of the first measurement.

We summarize the Bell states of entanglement and their generation, since this concept is generalized in the following section for the higher-radix case. In the case of maximally entangled qubit pairs, there are four cases with respect to the computational basis states referred to as the "Bell states" in honor of the the Bell inequalities [2]. The Bell states include

$$\begin{aligned} |B_{00}\rangle = |\Phi^+\rangle &= \tfrac{|00_2\rangle + |11_2\rangle}{\sqrt{2}}, \qquad |B_{01}\rangle = |\Psi^+\rangle = \tfrac{|01_2\rangle + |10_2\rangle}{\sqrt{2}}, \\ |B_{10}\rangle = |\Phi^-\rangle &= \tfrac{|00_2\rangle - |11_2\rangle}{\sqrt{2}}, \qquad |B_{11}\rangle = |\Psi^-\rangle = \tfrac{|01_2\rangle - |10_2\rangle}{\sqrt{2}}. \end{aligned} \tag{4}$$

The Bell states are inseparable in the sense that they cannot be expressed in terms of factors that contain expressions with only a single qubit. A "Bell state generator" is a QIP operator sequence that transforms two qubits in a basis state into one of the four maximally entangled Bell states. Although a number of different quantum circuits may be used to generate entangled qubits, a Bell state generator is most commonly described in the literature as being composed of a Hadamard and controlled-NOT ($\mathbf{C}_{NOT}$) operator as depicted in Figure 1. There are many other quantum circuits that can be used for Bell state generation with the same transfer matrix as that expressed by the Hadamard and $\mathbf{C}_{NOT}$ configuration. It is also possible to generate other arbitrary entangled pairs that are not maximally entangled. These non-maximally entangled states refer to the case where the non-zero probability amplitudes for the basis states have magnitude values that differ.

Definition 2.5 (Non-maximal Entanglement). When the coefficients of an entangled quantum state have non-equal values of squared magnitude for basis states, i.e., one of the basis states is more likely than another, the quantum state demonstrates non-maximal entanglement.

Entanglement is not limited to radix-2. Higher-ordered qudits of radix-3 and beyond can become entangled through initializing them into a basis state and then evolving them with an appropriate higher-radix entanglement generator. To generate qudits that are maximally entangled through a generalization of the Bell state generator of Figure 1, we use an operator that produces a maximally superimposed qudit analogous to the function of the Hadamard gate and operators with two-qudit interaction analogous to the $\mathbf{C}_{NOT}$.

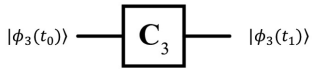

Fig. 2. Radix-3 Chrestenson gate, $\mathbf{C}_3$ evolving $|\phi_3\rangle$.

3 ENTANGLEMENT GENERATOR OPERATIONS

3.1 The Hadamard Gate

The Hadamard operator causes a qubit originally in a basis state to evolve into a maximally superimposed state and is denoted by the unitary transformation matrix **H**. Each column, or row, vector composing **H** is a discretized Walsh function with a scalar normalization factor of $\frac{1}{\sqrt{2^n}}$ where n is the order of the matrix that corresponds to the number of qubits composing the quantum system. Since the Walsh functions are orthogonal and the Hadamard transform matrix includes a scalar normalization factor, the overall **H** matrix is composed of an orthonormal column, or row, space. The first-order Hadamard matrix, **H**, is expressed as

$$\mathbf{H} = \frac{1}{\sqrt{2}} \begin{bmatrix} 1 & 1 \\ 1 & -1 \end{bmatrix}. \tag{5}$$

H evolves a qubit, $|\phi_2\rangle$, initially in a basis state, into a state of maximal superposition so it has equal probability of being observed, or measured, as either $|0_2\rangle$ or $|1_2\rangle$. As an example, consider the qubit $|\phi_2\rangle = |0_2\rangle$ that is evolved in time through application of a Hadamard operation, $|\phi_2\rangle = \mathbf{H}|0_2\rangle = (1/\sqrt{2})(|0\rangle + |1\rangle)$.

3.2 The Chrestenson Gate

In preparation for presenting our result that describes how entanglement states for higher-radix qudits can be generated, we present one of the crucial operators, the Chrestenson gate. Quantum operators exist for other computational bases, such as radix-3 and above, that achieve equal superposition among the corresponding basis states. These operators are referred to as "Chrestenson" gates. Since the Chrestenson operators can be formed for any radix $r > 2$, we denote them as $\mathbf{C}_r$ to indicate the radix, and alternatively, that $\mathbf{C}_r$ is a square matrix of dimension $r \times r$. Chrestenson gates are characterized by transformation matrices that may be derived using the discrete Fourier transform over Abelian groups. The general theory of the discrete Fourier transform over Abelian groups, referred to as the Chrestenson transform, can be found in References [9, 27]. Many useful applications of Chrestenson transforms in QIS have been demonstrated [28].

The graphical representation of the application of a Chrestenson gate, $\mathbf{C}_3$, on a radix-3 qudit at time t_0 is in Figure 2 and illustrates the operation $|\phi_3(t_1)\rangle = \mathbf{C}_3|\phi_3(t_0)\rangle$. Because the Chrestenson operator is a generalized version of the Hadamard operator wherein the radix, r, is an integer greater than two, the resulting transformation matrix for a single qudit is square with dimension $r \times r$. The Chrestenson transform can likewise be applied to a collection of n qudits with a resulting transformation matrix of dimension $r^n \times r^n$. The corresponding transformation matrix can be formed using the tensor product of n Chrestenson transformation matrices of dimension $r \times r$ and is denoted as

$$\mathbf{C}_r^n = \bigotimes_{i=1}^{n} \mathbf{C}_r = \mathbf{C}_r \otimes \mathbf{C}_r \otimes \cdots \otimes \mathbf{C}_r. \tag{6}$$

The structure of the Chrestenson transform matrix is in the form of a Vandermonde matrix where each row vector consists of component, w_k, raised to an integral power j. The components within a Chrestenson transform matrix, w_k, are one of the rth roots of unity raised to some integral power [9, 29]. The rth roots of unity may be geometrically envisioned as r points that lie upon the unit

circle in the complex plane that are equiangular and that always include the $(1, 0)$ point denoted as w_0 along the positive real axis. In general, for radix-r, the roots of unity of interest are denoted as w_k where $k = 0, 1, \ldots, (r-1)$ and satisfy $(w_k)^r = 1$ as roots of one. The closed form representation of the rth roots of unity is $w_k = e^{i\frac{2\pi}{r}\times k}$.

Regarding notation, each element of the matrix is some form of w_k^j where j is determined by the column index and k is determined by the row index. In this indexing scheme, the indices j and k begin with $j = k = 0$ and increase to $j = k = (r-1)$. It is observed that, for the case $r = 2$, the Hadamard matrix results. Thus, the Chrestenson transform matrices can be considered as generalizations of the Hadamard transform for higher-dimensioned systems. The generalized Chrestenson transform matrix, $\mathbf{C}_r$, is

$$\mathbf{C}_r = \frac{1}{\sqrt{r}} \begin{bmatrix} w_0^0 & w_0^1 & \cdots & w_0^{(r-1)} \\ w_1^0 & w_1^1 & \cdots & w_1^{(r-1)} \\ \vdots & \vdots & \ddots & \vdots \\ w_{(r-1)}^0 & w_{(r-1)}^1 & \cdots & w_{(r-1)}^{(r-1)} \end{bmatrix}. \tag{7}$$

The transformation matrix of Equation (7) is composed of a set of normalized orthogonal Chrestenson functions as the column or row vectors [9]. The Chrestenson gate has been physically implemented and an example implementation of the radix-4 Chrestenson gate can be found in References [23, 24]. As is similar to the Hadamard gate acting on a qubit, the radix-r Chrestenson gate evolves a radix-r qudit into a state of maximal superposition when the qudit is initialized to a basis state.

Example 3.1 (Radix-3 Chrestenson Transform). The $\mathbf{C}_3$ operator uses the third roots of unity, $w_0 = \exp[i(2\pi/3)\times 0] = 1, w_1 = \exp[i(2\pi/3)\times 1] = \frac{1}{2}(-1 + i\sqrt{3})$, and $w_2 = \exp[i(2\pi/3)\times 2] = \frac{1}{2}(-1 - i\sqrt{3})$, in the general form in Equation (7). Specifically, the radix-3 Chrestenson gate transformation matrix is

$$\mathbf{C}_3 = \frac{1}{\sqrt{3}} \begin{bmatrix} w_0^0 & w_0^1 & w_0^2 \\ w_1^0 & w_1^1 & w_1^2 \\ w_2^0 & w_2^1 & w_2^2 \end{bmatrix} = \frac{1}{\sqrt{3}} \begin{bmatrix} 1 & 1 & 1 \\ 1 & e^{\frac{i2\pi}{3}\times 1} & e^{\frac{i2\pi}{3}\times 2} \\ 1 & e^{\frac{i2\pi}{3}\times 2} & e^{\frac{i2\pi}{3}\times 4} \end{bmatrix}. \tag{8}$$

As an example, consider a radix-3 qudit represented by the quantum state, $|\phi_3(t_0)\rangle = a_0|0_3\rangle + a_1|1_3\rangle + a_2|2_3\rangle$, at time t_0. When this qudit is evolved via the application of a Chrestenson operator, the resulting quantum state vector, denoted as $|\phi_3(t_1)\rangle$, is calculated as

$$|\phi_3(t_1)\rangle = \mathbf{C}_3|\phi_3(t_0)\rangle = \frac{1}{\sqrt{3}} \begin{bmatrix} 1 & 1 & 1 \\ 1 & e^{\frac{i2\pi}{3}\times 1} & e^{\frac{i2\pi}{3}\times 2} \\ 1 & e^{\frac{i2\pi}{3}\times 2} & e^{\frac{i2\pi}{3}\times 4} \end{bmatrix} \begin{bmatrix} a_0 \\ a_1 \\ a_2 \end{bmatrix} = \frac{1}{\sqrt{3}} \begin{bmatrix} (a_0 + a_1 + a_2) \\ (a_0 + w_1 a_1 + w_2 a_2) \\ (a_0 + w_2 a_1 + w_1 a_2) \end{bmatrix}.$$

Next, consider the cases where the qudit $|\phi_3(t_0)\rangle$ is initially in one of the three computational basis states of $|0_3\rangle$, $|1_3\rangle$, or $|2_3\rangle$ at time t_0. The case where $|\phi_3\rangle$ is initialized to basis vector $|\phi_3(t_0)\rangle = |0_3\rangle$ will be examined. Application of the Chrestenson operator, $\mathbf{C}_3$, causes the evolved quantum state, $|\phi_3(t_1)\rangle$ to become maximally superimposed as shown in the following calculations

$$|\phi_3(t_1)\rangle = \mathbf{C}_3|\phi_3(t_0)\rangle = \frac{1}{\sqrt{3}} \begin{bmatrix} 1 & 1 & 1 \\ 1 & e^{\frac{i2\pi}{3}\times 1} & e^{\frac{i2\pi}{3}\times 2} \\ 1 & e^{\frac{i2\pi}{3}\times 2} & e^{\frac{i2\pi}{3}\times 4} \end{bmatrix} \begin{bmatrix} 1 \\ 0 \\ 0 \end{bmatrix} = \frac{1}{\sqrt{3}} \begin{bmatrix} 1 \\ 1 \\ 1 \end{bmatrix} = \frac{|0_3\rangle + |1_3\rangle + |2_3\rangle}{\sqrt{3}}.$$

Applying Born's rule, it is observed that the probability of observing $|\phi_3(t_1)\rangle$ as being in any of the three basis states is equal,

$$Prob[|\phi_3(t_1)\rangle = |0_3\rangle] = Prob[|\phi_3(t_1)\rangle = |1_3\rangle] = Prob[|\phi_3(t_1)\rangle = |2_3\rangle] = \left|\left(\frac{1}{\sqrt{3}}\right)\right|^2 = \frac{1}{3}.$$

To summarize and for completeness, the well-known formal result is that the application of a radix-r Chrestenson operator to a radix-r qudit in a basis state results in a maximally superimposed qudit in Lemma 3.2.

Lemma 3.2 (Maximal Superposition Generation). *When a qudit is initialized to a basis state, it can be evolved to a state of maximal superposition via the application of the radix-r Chrestenson transform.*

Proof. When a qudit is initialized to a basis state, it can be expressed as the r-dimensional column vector $|i\rangle$ where i is an integer value in the set $\{0, 1, \ldots, (r-1)\}$ and furthermore where all components of $|i\rangle$ are zero except the singular ith component that has unity value.

The evolution of $|i\rangle$ due to the Chrestenson operator $\mathbf{C}_r$ is $\mathbf{C}_r|i\rangle = |c_i\rangle$. The evolved quantum state, $|c_i\rangle$, is identical to the ith column vector of the Chrestenson transformation matrix $\mathbf{C}_r$. By inspection of the structure of $\mathbf{C}_r$ as given in Equation (7), and due to the fact that each element of $|c_i\rangle$ is the ith power of each of the r different and unique rth roots of unity divided by the constant $\frac{1}{\sqrt{r}}$, it is observed that the evolved quantum state $|c_i\rangle$ is maximally superimposed, since the evolved state is a linear combination of all basis vectors with a magnitude of $\frac{1}{\sqrt{r}}$. □

3.3 Controlled Modulo-add Operations

In preparation for presenting our result that describes how entangled states for higher-radix qudits can be generated, we present one of the crucial operators, the family of controlled-modulo-addition gates. The radix-2 **X** operation, or **NOT** operation, performs a Pauli-**X** rotation on a qubit. Mathematically, the Pauli-**X** operation can be considered a modulo-2 addition-by-one operation as it evolves a qubit $|0_2\rangle$ to be $|((0+1)\text{mod } 2)_2\rangle = |1_2\rangle$ and $|1_2\rangle$ to $|((1+1)\text{mod } 2)_2\rangle = |0_2\rangle$. In the case where $|\phi_2\rangle$ is in a state of superposition, $|\phi_2(t_0)\rangle = a_0|0_2\rangle + a_1|1_2\rangle$, the **X** operation exchanges the probability amplitude coefficients of the quantum state yielding the qubit $|\phi_2(t_1)\rangle = a_1|0_2\rangle + a_0|1_2\rangle$. The quantum gate or operator for the Pauli-**X** is represented with the transformation matrix

$$\mathbf{X} = \begin{bmatrix} 0 & 1 \\ 1 & 0 \end{bmatrix}. \tag{9}$$

The controlled version of the **X** gate is the "controlled-**X**" or "controlled-NOT" gate denoted as $\mathbf{C}_{NOT}$. For consistency with the remainder of this article, the controlled-NOT gate may also be referred to by the somewhat unconventional name of "controlled-modulo-add by one" gate for reasons that will become apparent in following sections. The $\mathbf{C}_{NOT}$ gate is defined as

$$\mathbf{C}_{NOT} = \begin{bmatrix} 1 & 0 & 0 & 0 \\ 0 & 1 & 0 & 0 \\ 0 & 0 & 0 & 1 \\ 0 & 0 & 1 & 0 \end{bmatrix}. \tag{10}$$

The $\mathbf{C}_{NOT}$ gate causes a Pauli-**X** operation on a target qubit if the control has a probability amplitude for $|1_2\rangle$.

In the case of radix-2 systems, only two different modulo-2 additions are possible, since there are two computational basis vectors, $|0_2\rangle$ and $|1_2\rangle$. Furthermore, one of these is the trivial case

of modulo-2 addition-by-zero that results in the identity transformation matrix and is not of interest. Thus, there is only one single-qubit modulo-2 addition operation of interest, the Pauli-**X** operation. Likewise, there is only one two-qubit controlled-modulo-addition operation of interest, the controlled-**X** or $\mathbf{C}_{NOT}$. In the context of maximal entanglement generators, the subject of this work, a "permissible controlled modulo-addition operator," must be defined.

Definition 3.3 (Permissible Controlled Mod-add Operator). A controlled modulo-addition operator is *permissible* when the control value that activates the target modulo-addition operator is any basis state $|h\rangle$ where $h \in \{0, \ldots, (r-1)\}$ and the target modulo-addition-by-k operation is restricted to non-zero values of k where $k \in \{1, \ldots, (r-1)\}$. Since the modulo-r addition-by-zero operation results in the radix-r identity transformation matrix, $\mathbf{I}_r$, controlled modulo-r addition-by-zero gates are considered trivial.

For the sake of completeness, it is noted that the single $r = 2$ controlled modulo-addition operation of interest, $\mathbf{C}_{NOT}$ could be considered to represent two different operations, since the "control" qubit may cause the target Pauli-**X** operation to occur when the control qubit is either $|1_2\rangle$ or $|0_2\rangle$. Most past work in binary QIS consider only the single $\mathbf{C}_{NOT}$ operator wherein the target is activated when the control is $|1_2\rangle$. If the other case is of interest, then it is represented as the $\mathbf{C}_{NOT}$ with the control qubit passing through a pair of Pauli-**X** operations, one before and one after the $\mathbf{C}_{NOT}$, to cause the target to activate when the control has value $|0_2\rangle$. However, for consistency, these two cases for $r = 2$ are considered, since the generalized controlled modulo-additions operations for qudits where $r > 2$ that are discussed later do consider different values of the control qudits that activate the target operation.

The single qudit modulo-addition operations are denoted as $\mathbf{M}_k$ for operators that cause a modulo-k addition with respect to modulus r as was used in Reference [26]. As is the case with qubits (*i.e.*, $r = 2$), the modulo-0 operation is equal to the identity function, or $\mathbf{M}_0 = \mathbf{I}_r$ where $\mathbf{I}_r$ is the $r \times r$ identity matrix. Later in this article, $\mathbf{M}_0$ may be used within equations rather than $\mathbf{I}_r$ to show patterns within quantum entanglement generator transformation functions. Using the $\mathbf{M}_k$ notation, the Pauli-**X** operator for qubits is $\mathbf{M}_1$.

Example 3.4 (Modulo-addition Operators for Radix-3). To demonstrate the non-trivial single qudit modulo-addition operations in the ternary, $r = 3$, case, consider the transformation matrices

$$\mathbf{M}_1 = \begin{bmatrix} 0 & 0 & 1 \\ 1 & 0 & 0 \\ 0 & 1 & 0 \end{bmatrix}, \quad \mathbf{M}_2 = \begin{bmatrix} 0 & 1 & 0 \\ 0 & 0 & 1 \\ 1 & 0 & 0 \end{bmatrix}. \tag{11}$$

The $\mathbf{M}_1$ operator causes the evolutions $|0_3\rangle \rightarrow |1_3\rangle$, $|1_3\rangle \rightarrow |2_3\rangle$, and $|2_3\rangle \rightarrow |0_3\rangle$ to occur. Likewise, $\mathbf{M}_2$ results in $|0_3\rangle \rightarrow |2_3\rangle$, $|1_3\rangle \rightarrow |0_3\rangle$, and $|2_3\rangle \rightarrow |1_3\rangle$.

For higher-dimensional systems with radix-r, $r > 2$, there are $r - 1$ different single non-trivial qudit modulo-r additions and, thus, $r - 1$ controlled-modulo-addition operations of interest with respect to modulus r for a single basis control value. Considering all combinations of control values, r, as well as the different moduli, $r - 1$, there are a total of $r^2 - r$ different and non-trivial controlled-modulo-addition operators with all possible control values. Since the controlled-modulo-addition transformation matrices, $\mathbf{A}_{h,k}$, operate over two qudits of arbitrary radix r, they are of dimension $r^2 \times r^2$.

Definition 3.5 (Controlled Modulo-addition-by-k Operator). A controlled modulo-addition-by-k gate is a two-qudit gate specified as $\mathbf{A}_{h,k}$. The target modulo-addition-by-k operation occurs on the target qudit when, and only when, the control qudit has the appropriate value as specified by the gate as h. The k value defines the modulo-addition operator to occur on the target. Controlled

modulo-addition gates with multiple control and addition-by-k values are composite controlled-mod-add operators.

In general, the radix-r controlled modulo-addition-k matrices, $\mathbf{A}_{h,k}$ where h and k have single values, are in the form

$$\mathbf{A}_{h,k} = \begin{bmatrix} \mathbf{D}_0 & \mathbf{0}_r & \cdots & \cdots & \cdots & \cdots & \mathbf{0}_r \\ \mathbf{0}_r & \mathbf{D}_1 & \mathbf{0}_r & \cdots & \cdots & \cdots & \mathbf{0}_r \\ \vdots & \mathbf{0}_r & \ddots & \mathbf{0}_r & \cdots & \cdots & \mathbf{0}_r \\ \vdots & \vdots & \mathbf{0}_r & \mathbf{D}_j & \mathbf{0}_r & \cdots & \mathbf{0}_r \\ \vdots & \vdots & \vdots & \mathbf{0}_r & \ddots & \mathbf{0}_r & \vdots \\ \vdots & \vdots & \vdots & \vdots & \mathbf{0}_r & \ddots & \mathbf{0}_r \\ \mathbf{0}_r & \mathbf{0}_r & \mathbf{0}_r & \mathbf{0}_r & \cdots & \mathbf{0}_r & \mathbf{D}_{(r-1)} \end{bmatrix}, \qquad \mathbf{D}_i = \begin{cases} \mathbf{M}_0 = \mathbf{I}_r, & i \neq h \\ \mathbf{M}_k, & i = h. \end{cases} \tag{12}$$

In the equation above, each submatrix along the diagonal is denoted as $\mathbf{D}_i$ and is of dimension $r \times r$. The two-qudit controlled variation of the modulo-add gate, $\mathbf{A}_{h,k}$, only allows the modulo-addition by k operation to occur on the target whenever the control qudit is in state, $|h\rangle$. Of course, the control qudit can, in general, be in a superimposed state. For example, the transformation function,

$$\mathbf{A}_{0,1} = \left[\begin{array}{ccc:ccc:ccc} 0 & 0 & 1 & 0 & 0 & 0 & 0 & 0 & 0 \\ 1 & 0 & 0 & 0 & 0 & 0 & 0 & 0 & 0 \\ 0 & 1 & 0 & 0 & 0 & 0 & 0 & 0 & 0 \\ \hdashline 0 & 0 & 0 & 1 & 0 & 0 & 0 & 0 & 0 \\ 0 & 0 & 0 & 0 & 1 & 0 & 0 & 0 & 0 \\ 0 & 0 & 0 & 0 & 0 & 1 & 0 & 0 & 0 \\ \hdashline 0 & 0 & 0 & 0 & 0 & 0 & 1 & 0 & 0 \\ 0 & 0 & 0 & 0 & 0 & 0 & 0 & 1 & 0 \\ 0 & 0 & 0 & 0 & 0 & 0 & 0 & 0 & 1 \end{array}\right],$$

only allows the $\mathbf{M}_1$ operation to execute on the target if the control qudit has a value of $|0_3\rangle$. If the control qudit is either $|1_3\rangle$ or $|2_3\rangle$, then the target qudit remains unchanged. When a ternary basis is utilized, $r = 3$, there are a total of six non-trivial variations of the controlled modulo-add gate. These are denoted as $\mathbf{A}_{0,1}$, $\mathbf{A}_{0,2}$, $\mathbf{A}_{1,1}$, $\mathbf{A}_{1,2}$, $\mathbf{A}_{2,1}$, and $\mathbf{A}_{2,2}$. The transformation matrices for $\mathbf{A}_{0,2}$, $\mathbf{A}_{1,1}$, $\mathbf{A}_{1,2}$, $\mathbf{A}_{2,1}$, and $\mathbf{A}_{2,2}$ are

$$\mathbf{A}_{0,2} = \left[\begin{array}{ccc:ccc:ccc} 0 & 1 & 0 & 0 & 0 & 0 & 0 & 0 & 0 \\ 0 & 0 & 1 & 0 & 0 & 0 & 0 & 0 & 0 \\ 1 & 0 & 0 & 0 & 0 & 0 & 0 & 0 & 0 \\ \hdashline 0 & 0 & 0 & 1 & 0 & 0 & 0 & 0 & 0 \\ 0 & 0 & 0 & 0 & 1 & 0 & 0 & 0 & 0 \\ 0 & 0 & 0 & 0 & 0 & 1 & 0 & 0 & 0 \\ \hdashline 0 & 0 & 0 & 0 & 0 & 0 & 1 & 0 & 0 \\ 0 & 0 & 0 & 0 & 0 & 0 & 0 & 1 & 0 \\ 0 & 0 & 0 & 0 & 0 & 0 & 0 & 0 & 1 \end{array}\right], \mathbf{A}_{1,1} = \left[\begin{array}{ccc:ccc:ccc} 1 & 0 & 0 & 0 & 0 & 0 & 0 & 0 & 0 \\ 0 & 1 & 0 & 0 & 0 & 0 & 0 & 0 & 0 \\ 0 & 0 & 1 & 0 & 0 & 0 & 0 & 0 & 0 \\ \hdashline 0 & 0 & 0 & 0 & 0 & 1 & 0 & 0 & 0 \\ 0 & 0 & 0 & 1 & 0 & 0 & 0 & 0 & 0 \\ 0 & 0 & 0 & 0 & 1 & 0 & 0 & 0 & 0 \\ \hdashline 0 & 0 & 0 & 0 & 0 & 0 & 1 & 0 & 0 \\ 0 & 0 & 0 & 0 & 0 & 0 & 0 & 1 & 0 \\ 0 & 0 & 0 & 0 & 0 & 0 & 0 & 0 & 1 \end{array}\right], \mathbf{A}_{1,2} = \left[\begin{array}{ccc:ccc:ccc} 1 & 0 & 0 & 0 & 0 & 0 & 0 & 0 & 0 \\ 0 & 1 & 0 & 0 & 0 & 0 & 0 & 0 & 0 \\ 0 & 0 & 1 & 0 & 0 & 0 & 0 & 0 & 0 \\ \hdashline 0 & 0 & 0 & 0 & 1 & 0 & 0 & 0 & 0 \\ 0 & 0 & 0 & 0 & 0 & 1 & 0 & 0 & 0 \\ 0 & 0 & 0 & 1 & 0 & 0 & 0 & 0 & 0 \\ \hdashline 0 & 0 & 0 & 0 & 0 & 0 & 1 & 0 & 0 \\ 0 & 0 & 0 & 0 & 0 & 0 & 0 & 1 & 0 \\ 0 & 0 & 0 & 0 & 0 & 0 & 0 & 0 & 1 \end{array}\right],$$

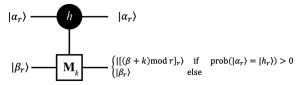

Fig. 3. Symbol of the controlled modulo-add gate, $\mathbf{A}_{h,k}$.

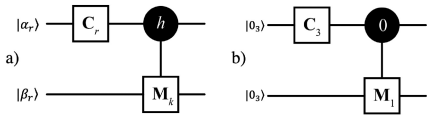

Fig. 4. (a) General circuit for radix-r two-qudit partial entanglement generator. (b) Specific example circuit for radix-3 two-qudit partial entanglement generator.

$$\mathbf{A}_{2,1} = \left[\begin{array}{ccc:ccc:ccc} 1&0&0&0&0&0&0&0&0\\ 0&1&0&0&0&0&0&0&0\\ 0&0&1&0&0&0&0&0&0\\ \hdashline 0&0&0&1&0&0&0&0&0\\ 0&0&0&0&1&0&0&0&0\\ 0&0&0&0&0&1&0&0&0\\ \hdashline 0&0&0&0&0&0&0&0&1\\ 0&0&0&0&0&0&1&0&0\\ 0&0&0&0&0&0&0&1&0 \end{array}\right], \mathbf{A}_{2,2} = \left[\begin{array}{ccc:ccc:ccc} 1&0&0&0&0&0&0&0&0\\ 0&1&0&0&0&0&0&0&0\\ 0&0&1&0&0&0&0&0&0\\ \hdashline 0&0&0&1&0&0&0&0&0\\ 0&0&0&0&1&0&0&0&0\\ 0&0&0&0&0&1&0&0&0\\ \hdashline 0&0&0&0&0&0&0&1&0\\ 0&0&0&0&0&0&0&0&1\\ 0&0&0&0&0&0&1&0&0 \end{array}\right].$$

The symbol for the generalized circuit for controlled modulo-add gate can be seen in Figure 3. In this generalized symbol, the h for the control qudit $|\alpha_r\rangle$ is the active control level that may have a value from the set $\{0, 1, \ldots, (r-1)\}$. Likewise, the target qudit $|\beta_r\rangle$ will be transformed by $\mathbf{M}_k$ where k has a value from the set $\{1, 2, \ldots, (r-1)\}$.

4 THE HIGHER-RADIX ENTANGLEMENT GENERATOR

Higher-radix quantum state generation has been considered in Reference [25] and maximal entanglement of QIP systems composed of radix-3, -4, and -5 have been considered in Reference [11]. This current work differs from past efforts, because entangled higher-radix systems are considered in a general sense, and the entanglement generators that are presented here theoretically extend to any arbitrary radix r. For brevity, $r = 3$ systems implementing two qudits are frequently used in examples, but our results also describe the methods to extend the entanglement generators into systems with more qudits.

4.1 Partial Entanglement of Qudit Pairs

In contrast to maximal entanglement, the state of partial entanglement must also be described. A partially entangled state is one wherein some subset of the basis states are entangled and the remaining set or sets are not. States of partial entanglement cannot exist in binary systems, $r = 2$, but they do exist for $r > 2$.

Using the structure of the well-known radix-2 Bell state generator as motivation, quantum generator circuits can be formulated as a cascade that includes a radix-r Chrestenson operator followed controlled modulo-add operator. This set of operations evolves a pair of qudits originally in a basis state into a partially, not maximally, entangled qudit pair. The general form of a particular radix-r partial entanglement generator is shown in Figure 4(a). There exist $r^2 - r$ different partial

Table 1. Outputs of Radix-3 Partial Entanglement Generator Circuit with $|0_3\rangle$ as Control Level

	Two-Qudit Gate in Generator	
Input	$\mathbf{A}_{0,1}$	$\mathbf{A}_{0,2}$
$\|00_3\rangle$	$\frac{1}{\sqrt{3}}(\|01_3\rangle + \|10_3\rangle + \|20_3\rangle)$	$\frac{1}{\sqrt{3}}(\|02_3\rangle + \|10_3\rangle + \|20_3\rangle)$
$\|01_3\rangle$	$\frac{1}{\sqrt{3}}(\|02_3\rangle + \|11_3\rangle + \|21_3\rangle)$	$\frac{1}{\sqrt{3}}(\|00_3\rangle + \|11_3\rangle + \|21_3\rangle)$
$\|02_3\rangle$	$\frac{1}{\sqrt{3}}(\|00_3\rangle + \|12_3\rangle + \|22_3\rangle)$	$\frac{1}{\sqrt{3}}(\|01_3\rangle + \|12_3\rangle + \|22_3\rangle)$
$\|10_3\rangle$	$\frac{1}{\sqrt{3}}\left(\|01_3\rangle + \frac{1}{2}(-1+i\sqrt{3})\|10_3\rangle + \frac{1}{2}(-1-i\sqrt{3})\|20_3\rangle\right)$	$\frac{1}{\sqrt{3}}\left(\|02_3\rangle + \frac{1}{2}(-1+i\sqrt{3})\|10_3\rangle + \frac{1}{2}(-1-i\sqrt{3})\|20_3\rangle\right)$
$\|11_3\rangle$	$\frac{1}{\sqrt{3}}\left(\|02_3\rangle + \frac{1}{2}(-1+i\sqrt{3})\|11_3\rangle + \frac{1}{2}(-1-i\sqrt{3})\|21_3\rangle\right)$	$\frac{1}{\sqrt{3}}\left(\|00_3\rangle + \frac{1}{2}(-1+i\sqrt{3})\|11_3\rangle + \frac{1}{2}(-1-i\sqrt{3})\|21_3\rangle\right)$
$\|12_3\rangle$	$\frac{1}{\sqrt{3}}\left(\|00_3\rangle + \frac{1}{2}(-1+i\sqrt{3})\|12_3\rangle + \frac{1}{2}(-1-i\sqrt{3})\|22_3\rangle\right)$	$\frac{1}{\sqrt{3}}\left(\|01_3\rangle + \frac{1}{2}(-1+i\sqrt{3})\|12_3\rangle + \frac{1}{2}(-1-i\sqrt{3})\|22_3\rangle\right)$
$\|20_3\rangle$	$\frac{1}{\sqrt{3}}\left(\|01_3\rangle + \frac{1}{2}(-1-i\sqrt{3})\|10_3\rangle + \frac{1}{2}(-1+i\sqrt{3})\|20_3\rangle\right)$	$\frac{1}{\sqrt{3}}\left(\|02_3\rangle + \frac{1}{2}(-1-i\sqrt{3})\|10_3\rangle + \frac{1}{2}(-1+i\sqrt{3})\|20_3\rangle\right)$
$\|21_3\rangle$	$\frac{1}{\sqrt{3}}\left(\|02_3\rangle + \frac{1}{2}(-1-i\sqrt{3})\|11_3\rangle + \frac{1}{2}(-1+i\sqrt{3})\|21_3\rangle\right)$	$\frac{1}{\sqrt{3}}\left(\|00_3\rangle + \frac{1}{2}(-1-i\sqrt{3})\|11_3\rangle + \frac{1}{2}(-1+i\sqrt{3})\|21_3\rangle\right)$
$\|22_3\rangle$	$\frac{1}{\sqrt{3}}\left(\|00_3\rangle + \frac{1}{2}(-1-i\sqrt{3})\|12_3\rangle + \frac{1}{2}(-1+i\sqrt{3})\|22_3\rangle\right)$	$\frac{1}{\sqrt{3}}\left(\|01_3\rangle + \frac{1}{2}(-1-i\sqrt{3})\|12_3\rangle + \frac{1}{2}(-1+i\sqrt{3})\|22_3\rangle\right)$

entanglement generators with a single controlled gate, as any non-trivial $\mathbf{A}_{h,k}$ operator can be used.

Example 4.1 (Radix-3 Partial Entanglement of Two Qudits). To illustrate the concept of partial entanglement, consider the case where $r = 3$ and a controlled-modulo add operator of the form $\mathbf{A}_{0,1}$ is utilized. Furthermore, assume that the initial quantum state of the radix-3 qudit pair is $|\alpha\beta_3\rangle = |00_3\rangle$. The specific partial entanglement generator is shown in Figure 4(b). The resulting partially entangled quantum state arising from the evolution of $|00_3\rangle$ through the radix-3 circuit of Figure 4(b) is calculated as $|\alpha\beta_3\rangle = \mathbf{T}_{par}|00_3\rangle$ where $\mathbf{T}_{par}$ is the transfer matrix of the partial entanglement generator. The partially entangled state is calculated as

$$\mathbf{T}_{par}|00_3\rangle = \mathbf{A}_{0,1}(\mathbf{C}_3 \otimes \mathbf{I}_3)|00_3\rangle = \frac{1}{\sqrt{3}}(|01_3\rangle + |10_3\rangle + |20_3\rangle) = \frac{1}{\sqrt{3}}[|01_3\rangle + (|1_3\rangle + |2_3\rangle) \otimes |0_3\rangle]. \tag{13}$$

Since the value $|0_3\rangle$ can be factored out of two of the three basis components in the evolved quantum state, the state is not fully entangled. However, this state is referenced as "partially entangled," since the state $|01_3\rangle$ is present. $|01_3\rangle$ can be considered an entangled basis state within the partially entangled output state in Equation (13), because measurement of either $|\alpha_3\rangle$ or $|\beta_3\rangle$ gives insight to the state of the other qudit. Thus, there is a probability of $\frac{1}{3}$ that an observation or measurement of the evolved state will be this entangled state. However, if the evolved form of qudit $|\beta_3\rangle$ is observed to be $|0_3\rangle$, then the evolved qudit $|\alpha_3\rangle$ may be either $|1_3\rangle$ or $|2_3\rangle$ with equal likelihood, thus violating the definition of maximal entanglement. Mathematically, partial entanglement is present due to the fact that $|0_3\rangle$ can be factored out of two of the components of the evolved state. In contrast, a maximally entangled state is one that has the characteristic where no such factoring is possible.

Because the radix-3 quantum logic has three basis states that can act as active control values for the controlled-mod-add operators and there are two non-trivial Modulo-add gates (i.e., $\mathbf{A}_{h,1}$ and $\mathbf{A}_{h,2}$ for $h \in \{0, 1, 2\}$), there are six different circuits that could potentially be used to create partial entanglement. The evolved states resulting from the radix-3 partial entanglement circuit can be seen in Table 1 where $|0_3\rangle$ is the control basis value, Table 2 where $|1_3\rangle$ is the control basis value, and Table 3 where $|2_3\rangle$ is the control basis value. In these tables, the control level allows either the modulo-add by one or Modulo-add by two function to act upon the target qudit. All of the states provided in these tables are only partially entangled, because a qudit can be factored out of a subset of the final quantum state's basis states, violating Definition 2.4.

Table 2. Outputs of Radix-3 Partial Entanglement Generator Circuit with $|1_3\rangle$ as Control Level

	Two-Qudit Gate in Generator	
Input	$\mathbf{A}_{1,1}$	$\mathbf{A}_{1,2}$
$\|00_3\rangle$	$\frac{1}{\sqrt{3}}(\|00_3\rangle + \|11_3\rangle + \|20_3\rangle)$	$\frac{1}{\sqrt{3}}(\|00_3\rangle + \|12_3\rangle + \|20_3\rangle)$
$\|01_3\rangle$	$\frac{1}{\sqrt{3}}(\|01_3\rangle + \|12_3\rangle + \|21_3\rangle)$	$\frac{1}{\sqrt{3}}(\|01_3\rangle + \|10_3\rangle + \|21_3\rangle)$
$\|02_3\rangle$	$\frac{1}{\sqrt{3}}(\|02_3\rangle + \|10_3\rangle + \|22_3\rangle)$	$\frac{1}{\sqrt{3}}(\|02_3\rangle + \|11_3\rangle + \|22_3\rangle)$
$\|10_3\rangle$	$\frac{1}{\sqrt{3}}\left(\|00_3\rangle + \frac{1}{2}(-1+i\sqrt{3})\|11_3\rangle + \frac{1}{2}(-1-i\sqrt{3})\|20_3\rangle\right)$	$\frac{1}{\sqrt{3}}\left(\|00_3\rangle + \frac{1}{2}(-1+i\sqrt{3})\|12_3\rangle + \frac{1}{2}(-1-i\sqrt{3})\|20_3\rangle\right)$
$\|11_3\rangle$	$\frac{1}{\sqrt{3}}\left(\|01_3\rangle + \frac{1}{2}(-1+i\sqrt{3})\|12_3\rangle + \frac{1}{2}(-1-i\sqrt{3})\|21_3\rangle\right)$	$\frac{1}{\sqrt{3}}\left(\|01_3\rangle + \frac{1}{2}(-1+i\sqrt{3})\|10_3\rangle + \frac{1}{2}(-1-i\sqrt{3})\|21_3\rangle\right)$
$\|12_3\rangle$	$\frac{1}{\sqrt{3}}\left(\|02_3\rangle + \frac{1}{2}(-1+i\sqrt{3})\|10_3\rangle + \frac{1}{2}(-1-i\sqrt{3})\|22_3\rangle\right)$	$\frac{1}{\sqrt{3}}\left(\|02_3\rangle + \frac{1}{2}(-1+i\sqrt{3})\|11_3\rangle + \frac{1}{2}(-1-i\sqrt{3})\|22_3\rangle\right)$
$\|20_3\rangle$	$\frac{1}{\sqrt{3}}\left(\|00_3\rangle + \frac{1}{2}(-1-i\sqrt{3})\|11_3\rangle + \frac{1}{2}(-1+i\sqrt{3})\|20_3\rangle\right)$	$\frac{1}{\sqrt{3}}\left(\|00_3\rangle + \frac{1}{2}(-1-i\sqrt{3})\|12_3\rangle + \frac{1}{2}(-1+i\sqrt{3})\|20_3\rangle\right)$
$\|21_3\rangle$	$\frac{1}{\sqrt{3}}\left(\|01_3\rangle + \frac{1}{2}(-1-i\sqrt{3})\|12_3\rangle + \frac{1}{2}(-1+i\sqrt{3})\|21_3\rangle\right)$	$\frac{1}{\sqrt{3}}\left(\|01_3\rangle + \frac{1}{2}(-1-i\sqrt{3})\|10_3\rangle + \frac{1}{2}(-1+i\sqrt{3})\|21_3\rangle\right)$
$\|22_3\rangle$	$\frac{1}{\sqrt{3}}\left(\|02_3\rangle + \frac{1}{2}(-1-i\sqrt{3})\|10_3\rangle + \frac{1}{2}(-1+i\sqrt{3})\|22_3\rangle\right)$	$\frac{1}{\sqrt{3}}\left(\|02_3\rangle + \frac{1}{2}(-1-i\sqrt{3})\|11_3\rangle + \frac{1}{2}(-1+i\sqrt{3})\|22_3\rangle\right)$

Table 3. Outputs of Radix-3 Partial Entanglement Generator Circuit with $|2_3\rangle$ as Control Level

	Two-Qudit Gate in Generator	
Input	$\mathbf{A}_{2,1}$	$\mathbf{A}_{2,2}$
$\|00_3\rangle$	$\frac{1}{\sqrt{3}}(\|00_3\rangle + \|10_3\rangle + \|21_3\rangle)$	$\frac{1}{\sqrt{3}}(\|00_3\rangle + \|10_3\rangle + \|22_3\rangle)$
$\|01_3\rangle$	$\frac{1}{\sqrt{3}}(\|01_3\rangle + \|11_3\rangle + \|22_3\rangle)$	$\frac{1}{\sqrt{3}}(\|01_3\rangle + \|11_3\rangle + \|20_3\rangle)$
$\|02_3\rangle$	$\frac{1}{\sqrt{3}}(\|02_3\rangle + \|12_3\rangle + \|20_3\rangle)$	$\frac{1}{\sqrt{3}}(\|02_3\rangle + \|12_3\rangle + \|21_3\rangle)$
$\|10_3\rangle$	$\frac{1}{\sqrt{3}}\left(\|00_3\rangle + \frac{1}{2}(-1+i\sqrt{3})\|10_3\rangle + \frac{1}{2}(-1-i\sqrt{3})\|21_3\rangle\right)$	$\frac{1}{\sqrt{3}}\left(\|00_3\rangle + \frac{1}{2}(-1+i\sqrt{3})\|10_3\rangle + \frac{1}{2}(-1-i\sqrt{3})\|22_3\rangle\right)$
$\|11_3\rangle$	$\frac{1}{\sqrt{3}}\left(\|01_3\rangle + \frac{1}{2}(-1+i\sqrt{3})\|11_3\rangle + \frac{1}{2}(-1-i\sqrt{3})\|22_3\rangle\right)$	$\frac{1}{\sqrt{3}}\left(\|01_3\rangle + \frac{1}{2}(-1+i\sqrt{3})\|11_3\rangle + \frac{1}{2}(-1-i\sqrt{3})\|20_3\rangle\right)$
$\|12_3\rangle$	$\frac{1}{\sqrt{3}}\left(\|02_3\rangle + \frac{1}{2}(-1+i\sqrt{3})\|12_3\rangle + \frac{1}{2}(-1-i\sqrt{3})\|20_3\rangle\right)$	$\frac{1}{\sqrt{3}}\left(\|02_3\rangle + \frac{1}{2}(-1+i\sqrt{3})\|12_3\rangle + \frac{1}{2}(-1-i\sqrt{3})\|21_3\rangle\right)$
$\|20_3\rangle$	$\frac{1}{\sqrt{3}}\left(\|00_3\rangle + \frac{1}{2}(-1-i\sqrt{3})\|10_3\rangle + \frac{1}{2}(-1+i\sqrt{3})\|21_3\rangle\right)$	$\frac{1}{\sqrt{3}}\left(\|00_3\rangle + \frac{1}{2}(-1-i\sqrt{3})\|10_3\rangle + \frac{1}{2}(-1+i\sqrt{3})\|22_3\rangle\right)$
$\|21_3\rangle$	$\frac{1}{\sqrt{3}}\left(\|01_3\rangle + \frac{1}{2}(-1-i\sqrt{3})\|11_3\rangle + \frac{1}{2}(-1+i\sqrt{3})\|22_3\rangle\right)$	$\frac{1}{\sqrt{3}}\left(\|01_3\rangle + \frac{1}{2}(-1-i\sqrt{3})\|11_3\rangle + \frac{1}{2}(-1+i\sqrt{3})\|20_3\rangle\right)$
$\|22_3\rangle$	$\frac{1}{\sqrt{3}}\left(\|02_3\rangle + \frac{1}{2}(-1-i\sqrt{3})\|12_3\rangle + \frac{1}{2}(-1+i\sqrt{3})\|20_3\rangle\right)$	$\frac{1}{\sqrt{3}}\left(\|02_3\rangle + \frac{1}{2}(-1-i\sqrt{3})\|12_3\rangle + \frac{1}{2}(-1+i\sqrt{3})\|21_3\rangle\right)$

4.2 Maximal Entanglement Generators for Qudit Pairs

Many radix-2 QIP algorithms begin with initializing the qubits in a ground or other basis state followed by placing them into states of full and maximal entanglement. This is accomplished by using a quantum circuit that includes the Hadamard gate and the $\mathbf{C}_{NOT}$, or radix-2 controlled-modulo-one, operator. If a quantum computer is a higher-radix device, then the analogous operation would be instantiated; that is, to first initialize all qudits into basis states and then to immediately perform Chrestenson operations to evolve the control qudits into states of maximal superposition. Next, specific controlled operations may be implemented to evolve the qudits into partial or maximal entanglement. Augmentations must be made to the circuit in Figure 4(a) to produce maximally entangled radix-r qudit pairs. A pair of radix-3 qudits can become maximally entangled when two controlled modulo-add operations are utilized rather than a single operation.

Example 4.2 (Maximal Entanglement Generator for Two Radix-3 Qudits). Fully entangling a pair of radix-3 qudits requires one additional controlled operation in the entanglement generator as compared to what is required for partial entanglement. The two controlled gates needed for full entanglement must have different target activation values, h, and they must have two different modulo-add by k operations on the target.

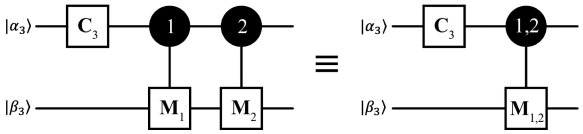

Fig. 5. Radix-3 two-qudit maximal entanglement generator implemented with $\mathbf{A}_{1,1}$ and $\mathbf{A}_{2,2}$ that form the composite gate $\mathbf{A}_{(1,2),(1,2)}$.

An example radix-3 full entanglement generator for two qudits can be seen in Figure 5. The transformation matrix for the controlled operations in the generator is derived by combining the single-control Modulo-add transformation functions, $\mathbf{A}_{1,1}$ in series with $\mathbf{A}_{2,2}$ using a matrix product. For example,

$$\mathbf{A}_{(1,2),(1,2)} = \mathbf{A}_{2,2} \times \mathbf{A}_{1,1} = \left[\begin{array}{ccc:ccc:ccc} 1&0&0&0&0&0&0&0&0\\ 0&1&0&0&0&0&0&0&0\\ 0&0&1&0&0&0&0&0&0\\ \hdashline 0&0&0&0&0&1&0&0&0\\ 0&0&0&1&0&0&0&0&0\\ 0&0&0&0&1&0&0&0&0\\ \hdashline 0&0&0&0&0&0&0&1&0\\ 0&0&0&0&0&0&0&0&1\\ 0&0&0&0&0&0&1&0&0 \end{array}\right] = \left[\begin{array}{ccc} \mathbf{M}_0 & \mathbf{0} & \mathbf{0}\\ \mathbf{0} & \mathbf{M}_1 & \mathbf{0}\\ \mathbf{0} & \mathbf{0} & \mathbf{M}_2 \end{array}\right] \tag{14}$$

is created by combining $\mathbf{A}_{2,2}$ with $\mathbf{A}_{1,1}$, and it describes the evolution associated with the entire controlled portion of Figure 5. Since combining the controlled-mod-add operations is commutative, the matrix products $\mathbf{A}_{2,2} \times \mathbf{A}_{1,1} = \mathbf{A}_{(1,2),(1,2)}$, $\mathbf{A}_{2,1} \times \mathbf{A}_{1,2} = \mathbf{A}_{(1,2),(2,1)}$, $\mathbf{A}_{2,2} \times \mathbf{A}_{0,1} = \mathbf{A}_{(0,2),(1,2)}$, $\mathbf{A}_{2,1} \times \mathbf{A}_{0,2} = \mathbf{A}_{(0,2),(2,1)}$, $\mathbf{A}_{1,2} \times \mathbf{A}_{0,1} = \mathbf{A}_{(0,1),(1,2)}$, and $\mathbf{A}_{1,1} \times \mathbf{A}_{0,2} = \mathbf{A}_{(0,1),(2,1)}$ describe all of the unique transformation functions that can be used as the multi-qudit gates of a radix-3 maximal entanglement generator for two qudits. All of the outputs created by these six different maximal entanglement generators are provided in Tables 4, 5, and 6. Table 4 contains information when $|1_3\rangle$ and $|2_3\rangle$ are the active control values, Table 5 contains information when $|0_3\rangle$ and $|2_3\rangle$ are the active controls, and Table 6 contains information when $|0_3\rangle$ and $|1_3\rangle$ are the active controls. If these tables are examined, then it is clear that they contain maximally entangled quantum states, since each qudit cannot be described independently from the pair. For example, the evolved state resulting from an initial state of $|00_3\rangle$ is provided in Table 4. The output qudit state corresponding to the input $|00_3\rangle$ for this maximum entanglement generator would be calculated as

$$\mathbf{T}_{max}|00_3\rangle = \mathbf{A}_{(1,2),(1,2)}(\mathbf{C}_3 \otimes \mathbf{I}_3)|00_3\rangle = \frac{1}{\sqrt{3}}(|00_3\rangle + |11_3\rangle + |22_3\rangle). \tag{15}$$

This generated state cannot be mathematically factored and can only be described as a summation of entangled basis states. Since the output of the two-qudit maximal entanglement generator agrees with Definition 2.4, the pair of radix-3 qudits are maximally entangled.

Figure 5 illustrates the maximal entanglement generator described in Example 4.2. In Figure 5, the two controlled-mod-add gates are shown as a single symbol in addition to two separate symbols. The composite and single transformation matrix in Equation (14) characterizes the controlled portion, $\mathbf{A}_{(1,2),(1,2)}$, of Figure 5. As previously discussed for a radix-3 two-qudit maximal entanglement generator, there are six different composite controlled-mod-add operators that can be implemented. These are the $\mathbf{A}_{(0,1),(1,2)}$, $\mathbf{A}_{(0,1),(2,1)}$, $\mathbf{A}_{(1,2),(1,2)}$, $\mathbf{A}_{(1,2),(2,1)}$, $\mathbf{A}_{(0,2),(1,2)}$, and $\mathbf{A}_{(0,2),(1,2)}$ operators.

Table 4. Outputs of Radix-3 Maximal Entanglement Generator Circuit with $|1_3\rangle$ and $|2_3\rangle$ as Control Levels

	Two-Qudit Gate in Generator	
Input	$\mathbf{A}_{2,2} \times \mathbf{A}_{1,1} = \mathbf{A}_{(1,2),(1,2)}$	$\mathbf{A}_{2,1} \times \mathbf{A}_{1,2} = \mathbf{A}_{(1,2),(2,1)}$
$\|00_3\rangle$	$\frac{1}{\sqrt{3}}(\|00_3\rangle + \|11_3\rangle + \|22_3\rangle)$	$\frac{1}{\sqrt{3}}(\|00_3\rangle + \|12_3\rangle + \|21_3\rangle)$
$\|01_3\rangle$	$\frac{1}{\sqrt{3}}(\|01_3\rangle + \|12_3\rangle + \|20_3\rangle)$	$\frac{1}{\sqrt{3}}(\|01_3\rangle + \|10_3\rangle + \|22_3\rangle)$
$\|02_3\rangle$	$\frac{1}{\sqrt{3}}(\|02_3\rangle + \|10_3\rangle + \|21_3\rangle)$	$\frac{1}{\sqrt{3}}(\|02_3\rangle + \|11_3\rangle + \|20_3\rangle)$
$\|10_3\rangle$	$\frac{1}{\sqrt{3}}\left(\|00_3\rangle + \frac{1}{2}(-1+i\sqrt{3})\|11_3\rangle + \frac{1}{2}(-1-i\sqrt{3})\|22_3\rangle\right)$	$\frac{1}{\sqrt{3}}\left(\|00_3\rangle + \frac{1}{2}(-1+i\sqrt{3})\|12_3\rangle + \frac{1}{2}(-1-i\sqrt{3})\|21_3\rangle\right)$
$\|11_3\rangle$	$\frac{1}{\sqrt{3}}\left(\|01_3\rangle + \frac{1}{2}(-1+i\sqrt{3})\|12_3\rangle + \frac{1}{2}(-1-i\sqrt{3})\|20_3\rangle\right)$	$\frac{1}{\sqrt{3}}\left(\|01_3\rangle + \frac{1}{2}(-1+i\sqrt{3})\|10_3\rangle + \frac{1}{2}(-1-i\sqrt{3})\|22_3\rangle\right)$
$\|12_3\rangle$	$\frac{1}{\sqrt{3}}\left(\|02_3\rangle + \frac{1}{2}(-1+i\sqrt{3})\|10_3\rangle + \frac{1}{2}(-1-i\sqrt{3})\|21_3\rangle\right)$	$\frac{1}{\sqrt{3}}\left(\|02_3\rangle + \frac{1}{2}(-1+i\sqrt{3})\|11_3\rangle + \frac{1}{2}(-1-i\sqrt{3})\|20_3\rangle\right)$
$\|20_3\rangle$	$\frac{1}{\sqrt{3}}\left(\|00_3\rangle + \frac{1}{2}(-1-i\sqrt{3})\|11_3\rangle + \frac{1}{2}(-1+i\sqrt{3})\|22_3\rangle\right)$	$\frac{1}{\sqrt{3}}\left(\|00_3\rangle + \frac{1}{2}(-1-i\sqrt{3})\|12_3\rangle + \frac{1}{2}(-1+i\sqrt{3})\|21_3\rangle\right)$
$\|21_3\rangle$	$\frac{1}{\sqrt{3}}\left(\|01_3\rangle + \frac{1}{2}(-1-i\sqrt{3})\|12_3\rangle + \frac{1}{2}(-1+i\sqrt{3})\|20_3\rangle\right)$	$\frac{1}{\sqrt{3}}\left(\|01_3\rangle + \frac{1}{2}(-1-i\sqrt{3})\|10_3\rangle + \frac{1}{2}(-1+i\sqrt{3})\|22_3\rangle\right)$
$\|22_3\rangle$	$\frac{1}{\sqrt{3}}\left(\|02_3\rangle + \frac{1}{2}(-1-i\sqrt{3})\|10_3\rangle + \frac{1}{2}(-1+i\sqrt{3})\|21_3\rangle\right)$	$\frac{1}{\sqrt{3}}\left(\|02_3\rangle + \frac{1}{2}(-1-i\sqrt{3})\|11_3\rangle + \frac{1}{2}(-1+i\sqrt{3})\|20_3\rangle\right)$

Table 5. Outputs of Radix-3 Maximal Entanglement Generator Circuit with $|0_3\rangle$ and $|2_3\rangle$ as Control Levels

	Two-Qudit Gate in Generator	
Input	$\mathbf{A}_{2,2} \times \mathbf{A}_{0,1} = \mathbf{A}_{(0,2),(1,2)}$	$\mathbf{A}_{2,1} \times \mathbf{A}_{0,2} = \mathbf{A}_{(0,2),(2,1)}$
$\|00_3\rangle$	$\frac{1}{\sqrt{3}}(\|01_3\rangle + \|10_3\rangle + \|22_3\rangle)$	$\frac{1}{\sqrt{3}}(\|02_3\rangle + \|10_3\rangle + \|21_3\rangle)$
$\|01_3\rangle$	$\frac{1}{\sqrt{3}}(\|02_3\rangle + \|11_3\rangle + \|20_3\rangle)$	$\frac{1}{\sqrt{3}}(\|00_3\rangle + \|11_3\rangle + \|22_3\rangle)$
$\|02_3\rangle$	$\frac{1}{\sqrt{3}}(\|00_3\rangle + \|12_3\rangle + \|21_3\rangle)$	$\frac{1}{\sqrt{3}}(\|01_3\rangle + \|12_3\rangle + \|20_3\rangle)$
$\|10_3\rangle$	$\frac{1}{\sqrt{3}}\left(\|01_3\rangle + \frac{1}{2}(-1+i\sqrt{3})\|10_3\rangle + \frac{1}{2}(-1-i\sqrt{3})\|22_3\rangle\right)$	$\frac{1}{\sqrt{3}}\left(\|02_3\rangle + \frac{1}{2}(-1+i\sqrt{3})\|10_3\rangle + \frac{1}{2}(-1-i\sqrt{3})\|21_3\rangle\right)$
$\|11_3\rangle$	$\frac{1}{\sqrt{3}}\left(\|02_3\rangle + \frac{1}{2}(-1+i\sqrt{3})\|11_3\rangle + \frac{1}{2}(-1-i\sqrt{3})\|20_3\rangle\right)$	$\frac{1}{\sqrt{3}}\left(\|00_3\rangle + \frac{1}{2}(-1+i\sqrt{3})\|11_3\rangle + \frac{1}{2}(-1-i\sqrt{3})\|22_3\rangle\right)$
$\|12_3\rangle$	$\frac{1}{\sqrt{3}}\left(\|00_3\rangle + \frac{1}{2}(-1+i\sqrt{3})\|12_3\rangle + \frac{1}{2}(-1-i\sqrt{3})\|21_3\rangle\right)$	$\frac{1}{\sqrt{3}}\left(\|01_3\rangle + \frac{1}{2}(-1+i\sqrt{3})\|12_3\rangle + \frac{1}{2}(-1-i\sqrt{3})\|20_3\rangle\right)$
$\|20_3\rangle$	$\frac{1}{\sqrt{3}}\left(\|01_3\rangle + \frac{1}{2}(-1-i\sqrt{3})\|10_3\rangle + \frac{1}{2}(-1+i\sqrt{3})\|22_3\rangle\right)$	$\frac{1}{\sqrt{3}}\left(\|02_3\rangle + \frac{1}{2}(-1-i\sqrt{3})\|10_3\rangle + \frac{1}{2}(-1+i\sqrt{3})\|21_3\rangle\right)$
$\|21_3\rangle$	$\frac{1}{\sqrt{3}}\left(\|02_3\rangle + \frac{1}{2}(-1-i\sqrt{3})\|11_3\rangle + \frac{1}{2}(-1+i\sqrt{3})\|20_3\rangle\right)$	$\frac{1}{\sqrt{3}}\left(\|00_3\rangle + \frac{1}{2}(-1-i\sqrt{3})\|11_3\rangle + \frac{1}{2}(-1+i\sqrt{3})\|22_3\rangle\right)$
$\|22_3\rangle$	$\frac{1}{\sqrt{3}}\left(\|00_3\rangle + \frac{1}{2}(-1-i\sqrt{3})\|12_3\rangle + \frac{1}{2}(-1+i\sqrt{3})\|21_3\rangle\right)$	$\frac{1}{\sqrt{3}}\left(\|01_3\rangle + \frac{1}{2}(-1-i\sqrt{3})\|12_3\rangle + \frac{1}{2}(-1+i\sqrt{3})\|20_3\rangle\right)$

Table 6. Outputs of Radix-3 Maximal Entanglement Generator Circuit with $|0_3\rangle$ and $|1_3\rangle$ as Control Levels

	Two-Qudit Gate in Generator	
Input	$\mathbf{A}_{1,2} \times \mathbf{A}_{0,1} = \mathbf{A}_{(0,1),(1,2)}$	$\mathbf{A}_{1,1} \times \mathbf{A}_{0,2} = \mathbf{A}_{(0,1),(2,1)}$
$\|00_3\rangle$	$\frac{1}{\sqrt{3}}(\|01_3\rangle + \|12_3\rangle + \|20_3\rangle)$	$\frac{1}{\sqrt{3}}(\|02_3\rangle + \|11_3\rangle + \|20_3\rangle)$
$\|01_3\rangle$	$\frac{1}{\sqrt{3}}(\|02_3\rangle + \|10_3\rangle + \|21_3\rangle)$	$\frac{1}{\sqrt{3}}(\|00_3\rangle + \|12_3\rangle + \|21_3\rangle)$
$\|02_3\rangle$	$\frac{1}{\sqrt{3}}(\|00_3\rangle + \|11_3\rangle + \|22_3\rangle)$	$\frac{1}{\sqrt{3}}(\|01_3\rangle + \|10_3\rangle + \|22_3\rangle)$
$\|10_3\rangle$	$\frac{1}{\sqrt{3}}\left(\|01_3\rangle + \frac{1}{2}(-1+i\sqrt{3})\|12_3\rangle + \frac{1}{2}(-1-i\sqrt{3})\|20_3\rangle\right)$	$\frac{1}{\sqrt{3}}\left(\|02_3\rangle + \frac{1}{2}(-1+i\sqrt{3})\|11_3\rangle + \frac{1}{2}(-1-i\sqrt{3})\|20_3\rangle\right)$
$\|11_3\rangle$	$\frac{1}{\sqrt{3}}\left(\|02_3\rangle + \frac{1}{2}(-1+i\sqrt{3})\|10_3\rangle + \frac{1}{2}(-1-i\sqrt{3})\|21_3\rangle\right)$	$\frac{1}{\sqrt{3}}\left(\|00_3\rangle + \frac{1}{2}(-1+i\sqrt{3})\|12_3\rangle + \frac{1}{2}(-1-i\sqrt{3})\|21_3\rangle\right)$
$\|12_3\rangle$	$\frac{1}{\sqrt{3}}\left(\|00_3\rangle + \frac{1}{2}(-1+i\sqrt{3})\|11_3\rangle + \frac{1}{2}(-1-i\sqrt{3})\|22_3\rangle\right)$	$\frac{1}{\sqrt{3}}\left(\|01_3\rangle + \frac{1}{2}(-1+i\sqrt{3})\|10_3\rangle + \frac{1}{2}(-1-i\sqrt{3})\|22_3\rangle\right)$
$\|20_3\rangle$	$\frac{1}{\sqrt{3}}\left(\|01_3\rangle + \frac{1}{2}(-1-i\sqrt{3})\|12_3\rangle + \frac{1}{2}(-1+i\sqrt{3})\|20_3\rangle\right)$	$\frac{1}{\sqrt{3}}\left(\|02_3\rangle + \frac{1}{2}(-1-i\sqrt{3})\|11_3\rangle + \frac{1}{2}(-1+i\sqrt{3})\|20_3\rangle\right)$
$\|21_3\rangle$	$\frac{1}{\sqrt{3}}\left(\|02_3\rangle + \frac{1}{2}(-1-i\sqrt{3})\|10_3\rangle + \frac{1}{2}(-1+i\sqrt{3})\|21_3\rangle\right)$	$\frac{1}{\sqrt{3}}\left(\|00_3\rangle + \frac{1}{2}(-1-i\sqrt{3})\|12_3\rangle + \frac{1}{2}(-1+i\sqrt{3})\|21_3\rangle\right)$
$\|22_3\rangle$	$\frac{1}{\sqrt{3}}\left(\|00_3\rangle + \frac{1}{2}(-1-i\sqrt{3})\|11_3\rangle + \frac{1}{2}(-1+i\sqrt{3})\|22_3\rangle\right)$	$\frac{1}{\sqrt{3}}\left(\|01_3\rangle + \frac{1}{2}(-1-i\sqrt{3})\|10_3\rangle + \frac{1}{2}(-1+i\sqrt{3})\|22_3\rangle\right)$

Observation of the radix-3 composite controlled-mod-add operators reveals a pattern. The structure of these operators that can be used in combination with a $\mathbf{C}_3$ Chrestenson gate to form a maximal entanglement generator is described in Lemma 4.3.

Lemma 4.3 (Radix-3 Composite Mod-add Operator). *A radix-3 maximal entanglement generator for two qudits can be formulated as a cascade of a single qudit Chrestenson operator, $\mathbf{C}_3$, and a composite controlled modulo-add operator, $\mathbf{A}_{(h_1,h_2),(k_1,k_2)}$. The qudit that is transformed by the Chrestenson operator acts as the control qudit. The generalized form of the composite controlled modulo-add operator, $\mathbf{A}_{(h_1,h_2),(k_1,k_2)}$, is defined as*

$$\mathbf{A}_{(h_1,h_2),(k_1,k_2)} = \begin{bmatrix} \mathbf{D}_0 & \mathbf{0}_3 & \mathbf{0}_3 \\ \mathbf{0}_3 & \mathbf{D}_1 & \mathbf{0}_3 \\ \mathbf{0}_3 & \mathbf{0}_3 & \mathbf{D}_2 \end{bmatrix}, \qquad \mathbf{D}_i = \begin{cases} \mathbf{M}_0, & i \neq h_1, h_2 \\ \mathbf{M}_{k_1}, & i = h_1 \\ \mathbf{M}_{k_2}, & i = h_2. \end{cases} \tag{16}$$

Proof. It is assumed that the entanglement generator evolves the quantum state $|\theta\phi_3(t_0)\rangle = |(i,j)_3\rangle$ where $(i,j) = \{0,1,2\} \times \{0,1,2\}$; that is, the initial quantum state is initialized to a basis state. It is further assumed without loss of generality that the control qudit is $|\theta_3\rangle$ and the target qudit is $|\phi_3\rangle$ when referring to the state evolution due to a controlled modulo-add operator.

A radix-3 controlled modulo-addition gate, $\mathbf{A}_{h_1,k_1}$, has the form as given in Equation (12), wherein it is a banded matrix and wherein the non-zero diagonal band is composed of matrices $\mathbf{B}_0$, $\mathbf{B}_1$, and $\mathbf{B}_2$ in the form

$$\mathbf{A}_{h,k} = \begin{bmatrix} \mathbf{B}_0 & \mathbf{0}_3 & \mathbf{0}_3 \\ \mathbf{0}_3 & \mathbf{B}_1 & \mathbf{0}_3 \\ \mathbf{0}_3 & \mathbf{0}_3 & \mathbf{B}_2 \end{bmatrix}.$$

From the definition of Equation (12), it is known that two of the set of 3×3 matrices $\mathbf{B}_0$, $\mathbf{B}_1$, and $\mathbf{B}_2$ are equivalent to $\mathbf{M}_0 = \mathbf{I}_3$. Furthermore, the $\mathbf{B}_i$ matrix that is not equivalent to $\mathbf{M}_0$ is equivalent to the single qudit modulo-addition-k matrix, $\mathbf{M}_{k_1}$.

It is assumed that the control qudit $|\theta_3\rangle$ is in a state of maximal superposition before it is applied to the controlled modulo-addition operators, as is consistent with the architecture of an entanglement generator. Thus, the control qudit $|\theta_3\rangle$ is mathematically in the form

$$|\theta_3\rangle = \frac{1}{\sqrt{3}}(|0_3\rangle + |1_3\rangle + |2_3\rangle),$$

with each basis multiplied by a radix-3 root of unity raised to some integral power depending on the control qudit's original value. Therefore, due to the control value h_1 of a controlled modulo-add operator, partial entanglement occurs between the $|(h_1)_3\rangle$ component of the control qudit $|\theta_3\rangle$ and the target qudit $|\phi_3\rangle$ due to the operation of $\mathbf{A}_{h_1,k_1}$ wherein the $|[(h_1), ((k_1 + \phi) \mod 3)]_3\rangle$ term becomes entangled only as is shown in the results of Tables 1, 2, and 3. Thus, the remaining $r - 1 = 3 - 1 = 2$ terms are not entangled.

To entangle the remaining $r - 1 = 2$ terms, it is necessary to apply another $\mathbf{A}_{h_2,k_2}$ operator such that $h_2 \neq h_1$ and $k_2 \neq k_1$ to ensure that non-entangled elements of the partially entangled quantum state are evolved. The result of this evolution causes the $|[(h_2), ((k_2 + \phi) \mod 3)]_3\rangle$ term to become entangled. Because two of the $r = 3$ terms are now entangled, the only possibility for the third term is for it to be in a fully entangled state also to satisfy Born's rule. Thus, the Lemma is proven. □

Another result of this theoretical study concerns the required number of controlled modulo-addition operators for a general radix-r maximal entanglement generator for two qudits where $r > 2$ is provided in Lemma 4.4.

Lemma 4.4 (Number of Mod-add Operators). *It is required that $r-1$ unique and permissible controlled-mod-add operators be utilized in a general maximal entanglement generator for two qudits wherein the controlling qudit is provided with a maximally superimposed state.*

Proof. It is well-known that a Bell state generator can be formed with a single Hadamard gate and a single C_{NOT} gate that can be considered to be a controlled modulo-addition-1 gate. This result indicates that maximal entanglement can be achieved for a system where $r = 2$ and the initial quantum state is a basis state when applied to the Bell state generator with $r - 1 = 2 - 1 = 1$ controlled modulo-addition operators.

Also, the result of Lemma 4.3 proved that for a radix-3 system, $r - 1 = 3 - 1 = 2$ controlled-modulo-add operators are required to achieve a state of maximal entanglement in an entanglement generator of the form wherein the control qudit $|\theta_3\rangle$ is in a state of maximal superposition and the target qudit $|\phi_3\rangle$ is initialized to a basis state.

By induction, it is the case that a maximal state generator for qudits of radix-r require the use of $r - 1$ controlled modulo-addition operators wherein the $r - 1$ controlled modulo-addition operators utilize control values that are mutually exclusive from the set $\{0, 1, 2, \ldots, (r - 1)\}$. Conditions for the the target modulo-addition operators, $\mathbf{M}_j$ are described as a result of the following Lemma 4.5. □

Lemma 4.5 (Unique Mod-add Operators). *A given radix-r two-qudit maximal entanglement generator is composed in part of $r - 1$ controlled modulo-addition operators wherein the operators are all non-trivial and permissible as defined in Definition 3.3 and furthermore wherein none of the operators are identical.*

Proof. Consider the group G where the group elements are all $r \times r$ permutation matrices $\mathbf{M}_i$ for $i \in \{0, 1, \ldots, (r - 1)\}$ and the group operator is direct matrix multiplication. Because G is a group, closure holds, thus $\mathbf{M}_i \times \mathbf{M}_i = \mathbf{M}_{(i+i)(\text{mod } r)} = \mathbf{M}_j$, where, $j = (i + i)(\text{mod } r)$.

Consider an attempted maximal entanglement generator composing in part $r - 1$ controlled modulo-addition operators wherein two of the $r - 1$ operators are identical and of the form $\mathbf{A}_{h,k}$.

Since the $\mathbf{M}_i$ permutation matrices in group G are identical to the modulo-addition-by-i transformation matrices in a controlled modulo-addition operator, this result indicates that the presence of two of the same $\mathbf{A}_{h,k}$ operators in a set of $r - 1$ operators composing an attempted maximal entanglement generator are equivalent to a set of $r - 2$ operators wherein the two identical $\mathbf{A}_{h,k}$ operators are equivalent to a single $\mathbf{A}_{h,2k(\text{mod } r)}$ operator.

From Lemma 4.4, it is proven that $r - 1$ unique and permissible controlled-mod-add operators be utilized. This requirement is violated when two identical controlled modulo-addition operators are present in the set of size $r - 1$, since two identical operators of the form $\mathbf{A}_{h,k}$ are equivalent to a single operator of the form $\mathbf{A}_{h,2k(\text{mod } r)}$. □

Generalizing Lemmas 4.3 and 4.4 leads to Theorem 4.6, which describes the requirements for the radix-r composite controlled-mod-add operators in a two-qudit maximal entanglement generator.

Theorem 4.6 (Entanglement Generator Control Operators). *The composite controlled mod-add operators in a radix-r maximal entanglement generator are a cascade of $r - 1$ permissible and unique controlled-mod-add operators of the form $\mathbf{A}_{h,k}$ where $h \in \{0, \ldots, (r - 1)\}$ and $k \in \{1, \ldots, (r - 1)\}$.*

Proof. From Lemma 4.4, $r - 1$ permissible controlled modulo-addition operators are required in a maximal entanglement generator for a pair of radix-r qudits. From Lemma 4.5, each of the $r - 1$ controlled modulo-addition operators must also be unique. Therefore, the theorem is proven. □

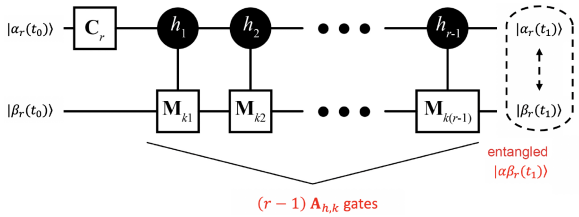

Fig. 6. Generalized maximal entanglement circuit for a radix-r qudit pair.

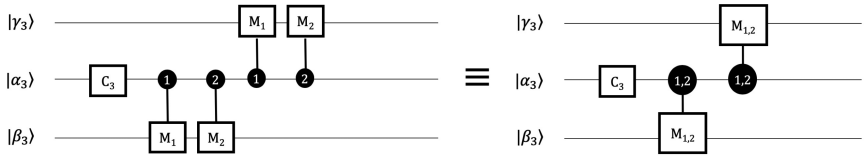

Fig. 7. Radix-3 three-qudit maximal entanglement generator implemented with two instances of $\mathbf{A}_{1,1} \times \mathbf{A}_{2,2} = \mathbf{A}_{(1,2),(1,2)}$.

These results lead to the main theoretical result of this article, the structure of a radix-r two-qudit maximal entanglement generator as provided in Corollary 4.7.

Corollary 4.7 (Entanglement Generator Structure). *The structure of a radix-r maximal entanglement generator for a radix-r qudit pair can be formed as a series of qudit evolutions in time wherein the first evolution is that resulting from the application of a radix-r Chrestenson gate to the first qudit. Then, the resulting evolved qudit controls the* $r-1$ *control inputs of the* $r-1$ *permissible and unique controlled modulo-addition gates where the second qudit acts as the target qudit on the* $r-1$ *controlled modulo-addition gates.*

Proof. From Lemma 3.2, a radix-r qudit initialized to a basis state is evolved to a state of maximal superposition when a radix-r Chrestenson transform is applied. Thus, a qudit in a basis state is maximally superimposed after it is evolved via a $\mathbf{C}_r$ Chrestenson gate. From Theorem 4.6, $r-1$ permissible and unique controlled modulo-addition operators are required in a radix-r maximal entanglement generator. Therefore, the corollary is proven. □

A generalized diagram of a radix-r maximal entanglement generator for two qudits is given in Figure 6.

4.3 Maximal Entanglement of Qudit Groups

The structure proven to entangle qudit pairs in Figure 6 extends into an even higher dimensional Hilbert space where the number of radix-r qudits is greater than two. The Bell state generator for radix-2 quantum logic can be expanded with an additional operator and qubit to produce GHZ states, which are states introduced in Reference [12] as examples of entanglement that involve at least three qubits. Similarly, the higher-radix maximal entanglement generator of this work is capable of entangling three qudits if minor modifications are made. An example of an $r = 3$, three-qudit maximal entanglement generator is pictured in Figure 7. It should be noted that many versions of the three-qudit generator can be created depending on the set of permissible controlled modulo-addition operators combined in a composite form to act on each target qudit.

Example 4.8 (Maximal Entanglement Generator for Three Radix-3 Qudits). By applying an additional set of $\mathbf{A}_{h,k}$ operators to an added qudit, the radix-3 two-qudit maximum entanglement generator of Figure 5 becomes the radix-3 three-qudit maximum entanglement generator pictured

Table 7. Outputs of radix-3 three-qudit maximal entanglement generator circuit in Figure 7

Input	Output
$\|000_3\rangle$	$\frac{1}{\sqrt{3}}\left(\|000_3\rangle + \|111_3\rangle + \|222_3\rangle\right)$
$\|001_3\rangle$	$\frac{1}{\sqrt{3}}\left(\|001_3\rangle + \|112_3\rangle + \|220_3\rangle\right)$
$\|002_3\rangle$	$\frac{1}{\sqrt{3}}\left(\|002_3\rangle + \|110_3\rangle + \|221_1\rangle\right)$
$\|010_3\rangle$	$\frac{1}{\sqrt{3}}\left(\|000_3\rangle + \frac{1}{2}(-1+i\sqrt{3})\|111_3\rangle + \frac{1}{2}(-1-i\sqrt{3})\|222_3\rangle\right)$
$\|011_3\rangle$	$\frac{1}{\sqrt{3}}\left(\|001_3\rangle + \frac{1}{2}(-1+i\sqrt{3})\|112_3\rangle + \frac{1}{2}(-1-i\sqrt{3})\|220_3\rangle\right)$
$\|012_3\rangle$	$\frac{1}{\sqrt{3}}\left(\|002_3\rangle + \frac{1}{2}(-1+i\sqrt{3})\|110_3\rangle + \frac{1}{2}(-1-i\sqrt{3})\|221_3\rangle\right)$
$\|020_3\rangle$	$\frac{1}{\sqrt{3}}\left(\|000_3\rangle + \frac{1}{2}(-1-i\sqrt{3})\|111_3\rangle + \frac{1}{2}(-1+i\sqrt{3})\|222_3\rangle\right)$
$\|021_3\rangle$	$\frac{1}{\sqrt{3}}\left(\|001_3\rangle + \frac{1}{2}(-1-i\sqrt{3})\|112_3\rangle + \frac{1}{2}(-1+i\sqrt{3})\|220_3\rangle\right)$
$\|022_3\rangle$	$\frac{1}{\sqrt{3}}\left(\|002_3\rangle + \frac{1}{2}(-1-i\sqrt{3})\|110_3\rangle + \frac{1}{2}(-1+i\sqrt{3})\|221_3\rangle\right)$
$\|100_3\rangle$	$\frac{1}{\sqrt{3}}\left(\|022_3\rangle + \|100_3\rangle + \|211_3\rangle\right)$
$\|101_3\rangle$	$\frac{1}{\sqrt{3}}\left(\|020_3\rangle + \|101_3\rangle + \|212_3\rangle\right)$
$\|102_3\rangle$	$\frac{1}{\sqrt{3}}\left(\|021_3\rangle + \|102_3\rangle + \|210_3\rangle\right)$
$\|110_3\rangle$	$\frac{1}{\sqrt{3}}\left(\frac{1}{2}(-1-i\sqrt{3})\|022_3\rangle + \|100_3\rangle + \frac{1}{2}(-1+i\sqrt{3})\|211_3\rangle\right)$
$\|111_3\rangle$	$\frac{1}{\sqrt{3}}\left(\frac{1}{2}(-1-i\sqrt{3})\|020_3\rangle + \|101_3\rangle + \frac{1}{2}(-1+i\sqrt{3})\|212_3\rangle\right)$
$\|112_3\rangle$	$\frac{1}{\sqrt{3}}\left(\frac{1}{2}(-1-i\sqrt{3})\|021_3\rangle + \|102_3\rangle + \frac{1}{2}(-1+i\sqrt{3})\|210_3\rangle\right)$
$\|120_3\rangle$	$\frac{1}{\sqrt{3}}\left(\frac{1}{2}(-1+i\sqrt{3})\|022_3\rangle + \|100_3\rangle + \frac{1}{2}(-1-i\sqrt{3})\|211_3\rangle\right)$
$\|121_3\rangle$	$\frac{1}{\sqrt{3}}\left(\frac{1}{2}(-1+i\sqrt{3})\|020_3\rangle + \|101_3\rangle + \frac{1}{2}(-1-i\sqrt{3})\|212_3\rangle\right)$
$\|122_3\rangle$	$\frac{1}{\sqrt{3}}\left(\frac{1}{2}(-1+i\sqrt{3})\|021_3\rangle + \|102_3\rangle + \frac{1}{2}(-1-i\sqrt{3})\|210_3\rangle\right)$
$\|200_3\rangle$	$\frac{1}{\sqrt{3}}\left(\|011_3\rangle + \|122_3\rangle + \|200_3\rangle\right)$
$\|201_3\rangle$	$\frac{1}{\sqrt{3}}\left(\|012_3\rangle + \|120_3\rangle + \|201_3\rangle\right)$
$\|202_3\rangle$	$\frac{1}{\sqrt{3}}\left(\|010_3\rangle + \|121_3\rangle + \|202_3\rangle\right)$
$\|210_3\rangle$	$\frac{1}{\sqrt{3}}\left(\frac{1}{2}(-1+i\sqrt{3})\|011_3\rangle + \frac{1}{2}(-1-i\sqrt{3})\|122_3\rangle + \|200_3\rangle\right)$
$\|211_3\rangle$	$\frac{1}{\sqrt{3}}\left(\frac{1}{2}(-1+i\sqrt{3})\|012_3\rangle + \frac{1}{2}(-1-i\sqrt{3})\|120_3\rangle + \|201_3\rangle\right)$
$\|212_3\rangle$	$\frac{1}{\sqrt{3}}\left(\frac{1}{2}(-1+i\sqrt{3})\|010_3\rangle + \frac{1}{2}(-1-i\sqrt{3})\|121_3\rangle + \|202_3\rangle\right)$
$\|220_3\rangle$	$\frac{1}{\sqrt{3}}\left(\frac{1}{2}(-1-i\sqrt{3})\|011_3\rangle + \frac{1}{2}(-1+i\sqrt{3})\|122_3\rangle + \|200_3\rangle\right)$
$\|221_3\rangle$	$\frac{1}{\sqrt{3}}\left(\frac{1}{2}(-1-i\sqrt{3})\|012_3\rangle + \frac{1}{2}(-1+i\sqrt{3})\|120_3\rangle + \|201_3\rangle\right)$
$\|222_3\rangle$	$\frac{1}{\sqrt{3}}\left(\frac{1}{2}(-1-i\sqrt{3})\|010_3\rangle + \frac{1}{2}(-1+i\sqrt{3})\|121_3\rangle + \|202_3\rangle\right)$

in Figure 7. In Figure 7 after the $\mathbf{C}_3$ gate acts on $|\alpha_3\rangle$, the $\mathbf{A}_{h,k}$ operators acting on $|\alpha_3\rangle$ and $|\beta_3\rangle$ are the same with respect to controls and modulo-adds as the operators acting on $|\alpha_3\rangle$ and $|\gamma_3\rangle$. The second set of gates acting on $|\alpha_3\rangle$ and $|\gamma_3\rangle$, however, are in a reversed orientation with the target qudit on the top qudit, $|\gamma_3\rangle$, and control qudit on the bottom qudit, $|\alpha_3\rangle$, and it should be noted that reversing the orientation of an operator causes an interchange of columns in the transformation matrix. A quantum operator $\mathbf{U}$ in its reversed orientation is indicated by $rev(\mathbf{U})$. This combination of gates causes $|\alpha_3\rangle$, $|\beta_3\rangle$, and $|\gamma_3\rangle$ to become entangled, as can be seen when the

state $|\gamma\alpha\beta_3\rangle = |000_3\rangle$ passes through the three-qudit maximal entanglement generator to create the output

$$\begin{aligned}\mathbf{T}_{max}|000_3\rangle &= (rev(\mathbf{A}_{(1,2),(1,2)}) \otimes \mathbf{I}_3)(\mathbf{I}_3 \otimes \mathbf{A}_{(1,2),(1,2)})(\mathbf{I}_3 \otimes \mathbf{C}_3 \otimes \mathbf{I}_3)|000_3\rangle \\ &= \frac{1}{\sqrt{3}}(|000_3\rangle + |111_3\rangle + |222_3\rangle). \end{aligned} \tag{17}$$

All of the three-qudit maximal entanglement generator outputs for the circuit in Figure 7 can be found in Table 7.

Within the scope of quantum entanglement of qudit groups, there are many additional topics that can be investigated to build on the work described here. For instance, although we have considered maximal entanglement generator structures capable of outputting GHZ-inspired states, we plan to generalize our methods in the future so they can output higher-radix quantum states inspired by W states where the number of basis states in the entanglement is greater than the system's radix r.

5 CONCLUSION

This article considers a generalization of the concept of maximally entangled qubits or EPR pairs for qudit pairs where the radix-r is a positive integer of the form $r > 2$. The concept of partial and maximal entanglement is presented, and it is shown that partial entanglement only exists for qudit pairs where $r > 2$. Entanglement generators are also devised for both partial and maximal entanglement when qudit pairs and qudit groups are initialized to basis states. These theoretical results should be of use to quantum computing algorithm designers when higher radix qudits are used as information carriers, and it is desired to generate maximally entangled qudits.

REFERENCES

[1] M. P. Almeida, S. P. Walborn, and P. H. Ribeiro. 2005. Four-dimensional quantum key distribution using position-momentum and polarization correlations. Retrieved from: *Arxiv Preprint Quant-ph/0510087* (2005).

[2] J. S. Bell. 1964. On the Einstein Podolsky Tosen paradox. *Phys. Physique Fiz.* 1 (Nov. 1964), 195–200. Issue 3. DOI : https://doi.org/10.1103/PhysicsPhysiqueFizika.1.195

[3] H. Bennett Ch and G. Brassard. 1984. Quantum cryptography: Public key distribution and coin tossing int. In *Proceedings of the Conference on Computers, Systems and Signal Processing*. 175–179.

[4] Mario Berta, Omar Fawzi, Volkher Scholz, and Oleg Szehr. 2014. Variations on classical and quantum extractors. In *Proceedings of the IEEE International Symposium on Information Theory (ISIT'14)*. IEEE, 1474–1478.

[5] Max Born. 1954. *The Statistical Interpretation of Quantum Mechanics*. Retrieved from: https://www.nobelprize.org/nobel_prizes/physics/laureates/1954/born-lecture.pdf.

[6] E. T. Burch, C. Henelsmith, W. Larson, and M. Beck. 2015. Quantum-state tomography of single-photon entangled states. *Phys. Rev. A* 92, 3 (2015), 032328.

[7] Davide Castelvecchi. 2017. Quantum computers ready to leap out of the lab in 2017. *Nat. News* 541, 7635 (2017), 9.

[8] Charles Q. Choi. 2017. Qudits: The real future of quantum computing? *IEEE Spect. Mag.* (2017). Retrieved on July 2018 from https://spectrum.ieee.org/tech-talk/computing/hardware/qudits-the-real-future-of-quantum-computing.

[9] H. E. Chrestenson et al. 1955. A class of generalized Walsh functions. *Pacific J. Math.* 5, 1 (1955), 17–31.

[10] Albert Einstein, Boris Podolsky, and Nathan Rosen. 1935. Can quantum-mechanical description of physical reality be considered complete? *Phys. Rev.* 47, 10 (1935), 777.

[11] M. Enríquez, I. Wintrowicz, and Karol Życzkowski. 2016. Maximally entangled multipartite states: A brief survey. In *J. Phys.: Conf. Series*, Vol. 698. IOP Publishing, 012003.

[12] Daniel M. Greenberger, Michael A. Horne, and Anton Zeilinger. 1989. Going beyond Bell's theorem. In *Bell's Theorem, Quantum Theory and Conceptions of the Universe*. Springer, 69–72.

[13] Lov K. Grover. 1996. A fast quantum mechanical algorithm for database search. In *Proceedings of the 28th ACM Symposium on Theory of Computing*. ACM, 212–219.

[14] Aram W. Harrow, Avinatan Hassidim, and Seth Lloyd. 2009. Quantum algorithm for linear systems of equations. *Phys. Rev. Lett.* 103, 15 (2009), 150502.

[15] Nurul Islam. 2018. *High-rate, High-dimensional Quantum Key Distribution Systems*. Ph.D. Dissertation. Duke University.
[16] Marco Lanzagorta. 2011. Quantum radar. *Synth. Lect. Quant. Comput.* 3, 1 (2011), 1–139.
[17] D. Michael Miller and Mitchell A. Thornton. 2007. Multiple valued logic: Concepts and representations. *Synth. Lect. Dig. Circ. Syst.* 2, 1 (2007), 1–127.
[18] Michael A. Nielsen and Isaac L. Chuang. 2010. *Quantum Computation and Quantum Information*. Cambridge University Press.
[19] Philipp Niemann, Rhitam Datta, and Robert Wille. 2016. Logic synthesis for quantum state generation. In *Proceedings of the IEEE 46th International Symposium on Multiple-Valued Logic (ISMVL'16)*. IEEE, 247–252.
[20] K. R. Rohit and Talabattula Srinivas. 2016. High dimensional quantum key distribution: BB84 protocol using qudits. In *Proceedings of the International Conference on Fibre Optics and Photonics*. Optical Society of America, Th3A–77.
[21] Roman Schmied. 2016. Quantum state tomography of a single qubit: Comparison of methods. *J. Mod. Optics* 63, 18 (2016), 1744–1758.
[22] Peter W. Shor. 1994. Algorithms for quantum computation: Discrete logarithms and factoring. In *Proceedings of the 35th Symposium on Foundations of Computer Science*. IEEE, 124–134.
[23] Kaitlin N. Smith, Tim P. LaFave, Duncan L. MacFarlane, and Mitchell A. Thornton. 2018. A radix-4 Chrestenson gate for optical quantum computation. In *Proceedings of the IEEE 48th International Symposium on Multiple-Valued Logic (ISMVL'18)*. IEEE.
[24] Kaitlin N. Smith, Tim P. LaFave Jr, Duncan L. MacFarlane, and Mitchell A. Thornton. 2018. Higher-radix Chrestenson gates for photonic quantum computation. *J. Appl. Log.* 5, 9 (2018), 1781–1798.
[25] R. T. Thew, Kae Nemoto, Andrew G. White, and William J. Munro. 2002. Qudit quantum-state tomography. *Phys. Rev. A* 66, 1 (2002), 012303.
[26] Mitchell A. Thornton, David W. Matula, Laura Spenner, and D. Michael Miller. 2008. Quantum logic implementation of unary arithmetic operations. In *Proceedings of the 38th International Symposium on Multiple Valued Logic (ISMVL'08)*. IEEE, 202–207.
[27] N. Ya Vilenkin. 1947. Concerning a class of complete orthogonal systems. In *Dokl. Akad. Nauk SSSR, Ser. Math.* Doklady Akademii Nauk SSSR.
[28] Zeljko Zilic and Katarzyna Radecka. 2002. The role of super-fast transforms in speeding up quantum computations. In *Proceedings of the 32nd IEEE International Symposium on Multiple-Valued Logic (ISMVL'02)*. IEEE, 129–135.
[29] Zeljko Zilic and Katarzyna Radecka. 2007. Scaling and better approximating quantum Fourier transform by higher radices. *IEEE Trans. Comput.* 56, 2 (2007), 202–207.

Received September 2018; revised May 2019; accepted July 2019